國立臺灣大學電機資訊學院生醫電子與資訊學研究所

碩士論文

Graduate Institute of Biomedical Electronics and Bioinformatics
College of Electrical Engineering and Computer Science
National Taiwan University

Master's Thesis

基於皮層－基底核－視丘迴路模擬對視覺刺激於巴金森氏症治療之機制研究

Investigate the therapeutic mechanism of visual stimulation on Parkinson's disease through cortical-basal ganglia-thalamic loop simulation

陳文碩

Wen-Shuo Chen

指導教授：林啟萬 博士

Advisor: Chii-Wann Lin Ph.D.

中華民國 113 年 4 月

April, 2024

doi:10.6342/NTU202400853

摘要

巴金森氏症（Parkinson’s disease）是一種影響中樞神經系統的慢性神經退化性疾病。目前，巴金森氏症的病理假說認為逐漸減少從緻密黑質部供應的多巴胺改變基底核神經元的放電模式並產生與巴金森氏症相關的β頻段異常震盪。在本研究中，我們透過建立了由 12 種基於 Hodgkin-Huxley 的神經元電導模型，進一步組成皮質－基底核－視丘迴路（cortical-basal ganglia-thalamic loop，CBT loop），以模擬皮質－基底核－視丘迴路在兩種不同生理與病理狀態組合下的表現，包含在不同的疾病嚴重程度（基線／輕度／中度／重度）和在不同的意識狀態（清醒／非快速動眼期／麻醉）。除此之外，我們也藉由模擬來比較深腦刺激術（deep brain stimulation）和視覺刺激如何影響巴金森氏症的皮質－基底核－視丘迴路的放電模式。本研究發現 1）視丘下核的深腦刺激術能完全阻斷視丘的上游訊號傳遞到其他下游腦區。2）視覺刺激能抑制視丘中的β頻段異常震盪並將正常的訊號傳遞到其他下游腦區。

關鍵字：巴金森氏症、皮層－基底核－視丘迴路、晝夜節律、非快速眼動睡眠、propofol 麻醉、腦深層刺激術、視覺刺激

doi:10.6342/NTU202400853

Abstract

Parkinson's disease (PD) is a chronic neurodegenerative disease affecting the central nervous system. The current pathological hypothesis suggests that the loss of dopaminergic input from substantia nigra pars compacta (SNc) altered basal ganglia neurons' firing pattern and eventually led to the emergence of a pathological beta band. Here, we build a whole Hodgkin-Huxley (HH) neuron-based cortical-basal ganglia-thalamic (CBT) loop model with twelve neuronal types as a library to simulate a combination of states, including PD progression states and cross-consciousness states. The simulation states include combinations of baseline (healthy)/three stages of PD and wake/non-rapid eye movement sleep/anesthesia. We also compare how deep brain stimulation (DBS) and visual stimulation affect the CBT loop dynamics in PD in silico. Our model shows that 1) subthalamic nucleus DBS can block all signals to further propagate from thalamic relay nuclei to other downstream circuitry. 2) optical stimulation can overcome the pathological beta wave in resting, wake thalamus, and propagate the desired signal to downstream circuitry.

Keywords: Parkinson’s disease (PD), cortical-basal ganglia-thalamic (CBT) loop, circadian rhythm, non-rapid eye movement (NREM), propofol anesthesia, deep brain stimulation (DBS), visual stimulation

doi:10.6342/NTU202400853

Contents

doi:10.6342/NTU202400853

List of Figures

List of Tables

doi:10.6342/NTU202400853

Chapter 1 Introduction

1.1 Parkinson's disease

Parkinson's disease (PD) is a chronic neurodegenerative disease affecting the central nervous system [1]. The incidence cases of PD are around 10 million people worldwide [2], about 1 million people in the U.S. [3] and 32000 in Taiwan [4]. The incidence rate of PD in the U.S. is 1% for the population over the age of 60 and 5% for the population over the age of 85 [5]. Besides, there are about 90000 people in the U.S. diagnosed with PD each year [3].

The current pathological hypothesis suggests that the loss of dopaminergic input from substantia nigra pars compacta (SNc) to basal ganglia altered basal ganglia neurons' firing pattern and eventually led to the emergence of a pathological beta band (13 to 30 Hz) [6], [7]. The impairment of dopamine production causes movement disorders, which include tremors, rigidity, bradykinesia, and postural instability [8], [9]. Other symptoms may include depression and other emotional changes, difficulty swallowing, chewing, speaking, urinary problems or constipation;, skin problems, and sleep disruptions [9].

Although PD is incurable, medicines, surgical treatment, and other therapies can often relieve and mitigate some symptoms. The most common medical treatment for PD is levodopa (L-dopa, a dopamine precursor), which can cross the blood-brain barrier (BBB) and be further converted into dopamine inside neurons to reverse declined dopamine levels [10]. However, long-term levodopa administration can provoke motor complications, such as levodopa-induced dyskinesia, tremors, and motor fluctuations. As

doi:10.6342/NTU202400853

disease progression deteriorates, levodopa efficacy declines, and thus needs to raise the dosage, which causes severe adverse effects [10]. Therefore, high-frequency (>100 Hz) deep brain stimulation (DBS), which has been shown to regulate the downstream of the stimulated nucleus, is introduced in the late stage of PD. Aside from traditional therapies, research suggests that rhythmic sensory stimulation (auditory and visual) can relieve PD movement disorders [11]. Furthermore, a recent study shows that external photo-modulation, e.g., 40 Hz visual stimulation, can help to raise gamma oscillations and might be a potential noninvasive and neuroprotection therapy against Alzheimer disease [12]. Although visual stimulus does not directly project from visual cortex to motor cortex (**Figure 1**) [13], the information might pass to the motor cortex through cortico-basal ganglia-thalamic (CBT) loop according to the neural pathway studies done by Foster et al. [14, Fig. 4].

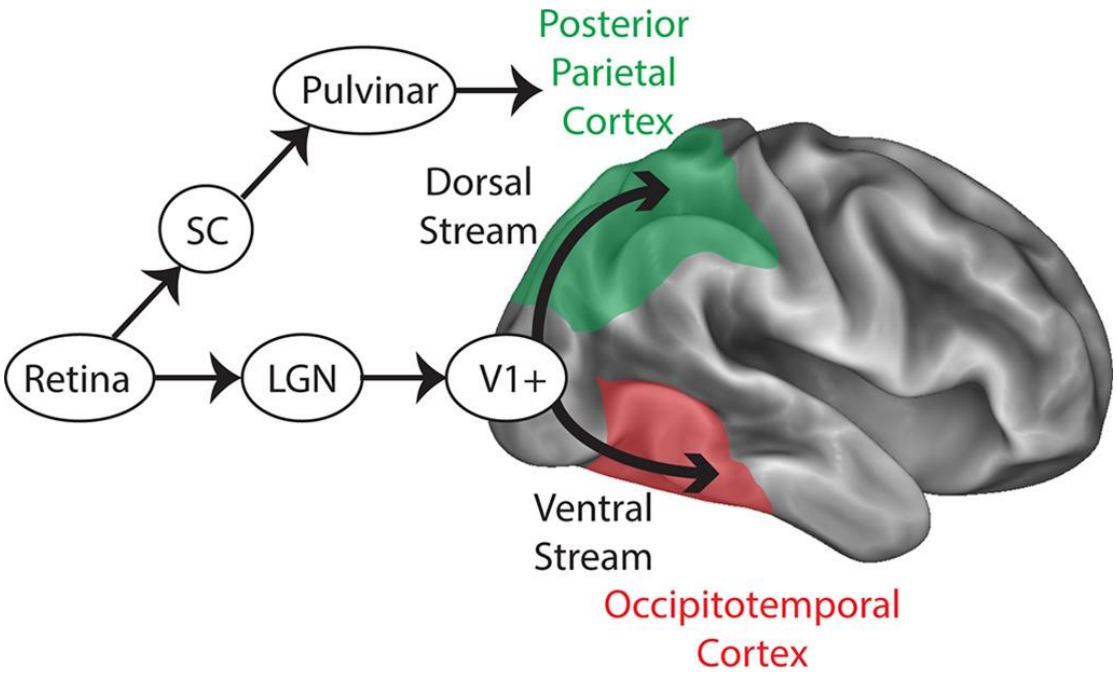

Figure 1: Visual stimulus from retina to posterior parietal cortex [13]
The visual information received in retina can be relayed to posterior parietal cortex (PPC) through superior colliculus (SC) route or visual pathway. The visual pathway starts from retina, lateral geniculate nucleus (LGN), primary visual cortex (V1) and finally to early visual areas (V1+). The information from V1+ then projects to PPC through dorsal stream

doi:10.6342/NTU202400853

(green). The other route from V1+ to occipitotemporal cortex is ventral stream (red).

The cortico-basal ganglia-thalamic (CBT) loop (**Figure 2**) has so far gained much attention since it's strongly related to many movement and neuropsychiatric disorders, including PD [15]. Understanding CBT loop dynamics through mathematical simulation could help us further explore PD pathological mechanisms and validate treatment efficacy.

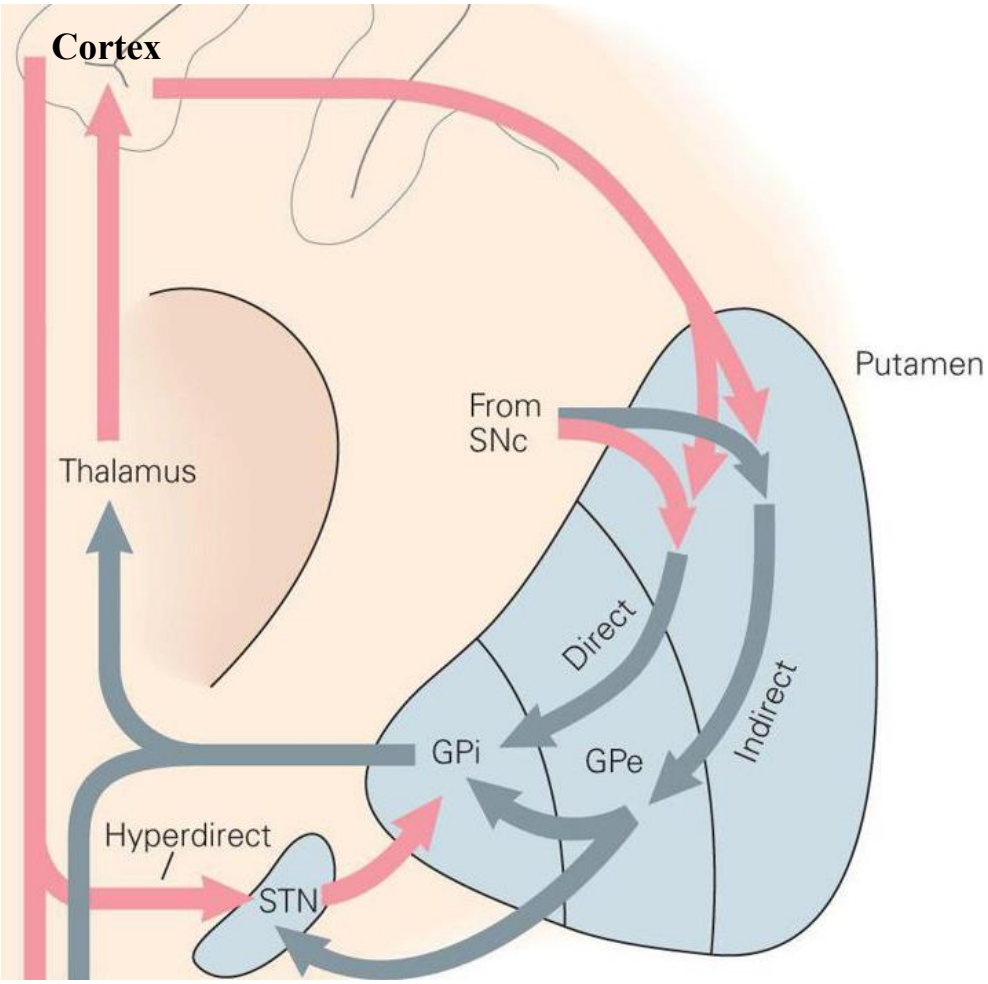

Figure 2: Cortico-basal ganglia-thalamic loop [16]
The loop contains two sub-loops: the thalamocortical loop and the basal-ganglia loop. Striatum (caudate and putamen in primates), globus pallidus (GPe: externus; GPi: internus), subthalamic nucleus (STN), and substantia nigra (SNr: pars reticulata; SNc: pars compacta).

doi:10.6342/NTU202400853

1.2 Thalamocortical loop

The thalamocortical loop involves various activities, including consciousness [17], learning (perceptual and associative) [18], short-term memory [19], circadian activities [20], etc. Circadian activities are regulated by the sleep-wake cycle. During the wake period, the Thalamocortical loop generates EEG waves containing nearly all frequency bands, including delta (0-4 Hz), theta (4-8 Hz), alpha (8-13 Hz), beta (13-30 Hz), gamma (30-80 Hz). While in the non-rapid eye movement (NREM) sleep period, neurons within loop activity are highly synchronized, and its EEG wave falls to a slow wave range (~2 Hz) [21, Fig. 2].

The thalamocortical loop consists of the cortex and thalamus. Afferent/encoded information (including perceptual information and preprocessed information from the lower-level cortex) first converges into the thalamus. The thalamus then decides to relay/decode the information back to cortical areas. Furthermore, recent studies raise the hypothesis that the loop works as neuronal phase-locked loops, which can recode the encoded information [22].

The cortex contains three dominant types of neurons: cortical pyramidal cells (PY), cortical fast-spiking interneurons (cFS), and cortical low-threshold spiking interneurons (LTS). The thalamus contains two dominant types of neurons: thalamic relay cells (TC) and thalamic reticular cells (RE). For each cortical module, PY receives TC excitatory pulses and receives local interneurons (cFS and LTS) inhibitory pulses; cFS or LTS receives TC and PY excitatory pulses and receives other cFS or LTS inhibitory pulses. TC gathers PY excitatory and RE inhibitory pulses and excites PY, TC, and RE. RE

doi:10.6342/NTU202400853

receives excitatory pulses from PY and TC, inhibiting TC and other RE [23].

During PD progression, the pathological beta wave is shown in PY regardless of wake or NREM sleep. Although NREM sleep is disrupted in PD and causes pathological beta wave emergence [21], no evidence exists that neurons within the loop have neuronal or synaptic changes. Therefore, the pathological beta wave might have originated from outer loop elements.

1.3 Basal ganglia loop

The striatum contains two major types of neurons: medium spiny neurons (MSN) and striatal fast-spiking interneurons (sFS). MSN occupy 90-95% of total striatum neurons [24]. MSN receives inputs from cortex (glutamatergic), thalamus (glutamatergic), other MSN (GABAergic), and striatal interneurons (regardless of GABAergic and cholinergic). MSN can be equally divided into two groups by the dopamine receptor types it contains. MSN with D1 type dopamine receptor (dMSN) output to SNr/GPi, known as a direct pathway. MSN with D2 type dopamine receptor (iMSN) first output to GPe, then to Subthalamic nucleus (STN), and finally to SNr/GPi, an indirect pathway. These two pathways compete with each other and are known as “Go” and “Not Go” in action selection [25].

sFS are the primary GABAergic striatal interneurons, making up 1% of total striatal neurons [26], [27]. sFS receives input from the cortex and thalamus—sFS output equally to nearby dMSN and iMSN, which forms feedforward inhibition circuitry. Aside from Parvalbumin+ sFS, NPY+ interneurons are primary cholinergic striatal interneurons

doi:10.6342/NTU202400853

whose activities are correlated to behavior [28]. Therefore, to reduce the complexity of the model, NPY+ interneurons-induced disinhibition on MSN is neglected.

During PD progression, the whole basal ganglia gradually lose dopamine input from SNc. dMSN is depressed, and iMSN is potentiated after dopamine depletion, which disturbs the balance between direct and indirect pathways (**Figure 3**) [29]. To maintain the homeostasis between the pathways, the shrinkage of dendritic spines of iMSN happens earlier than of dMSN. As for sFS, dopamine depletion does not affect sFS population size or responsiveness of cortical input. The change of synaptic strength of sFS to dMSN and iMSN in early PD is controversial, probably due to multiple mechanisms to suppress indirect pathways [29], [30].

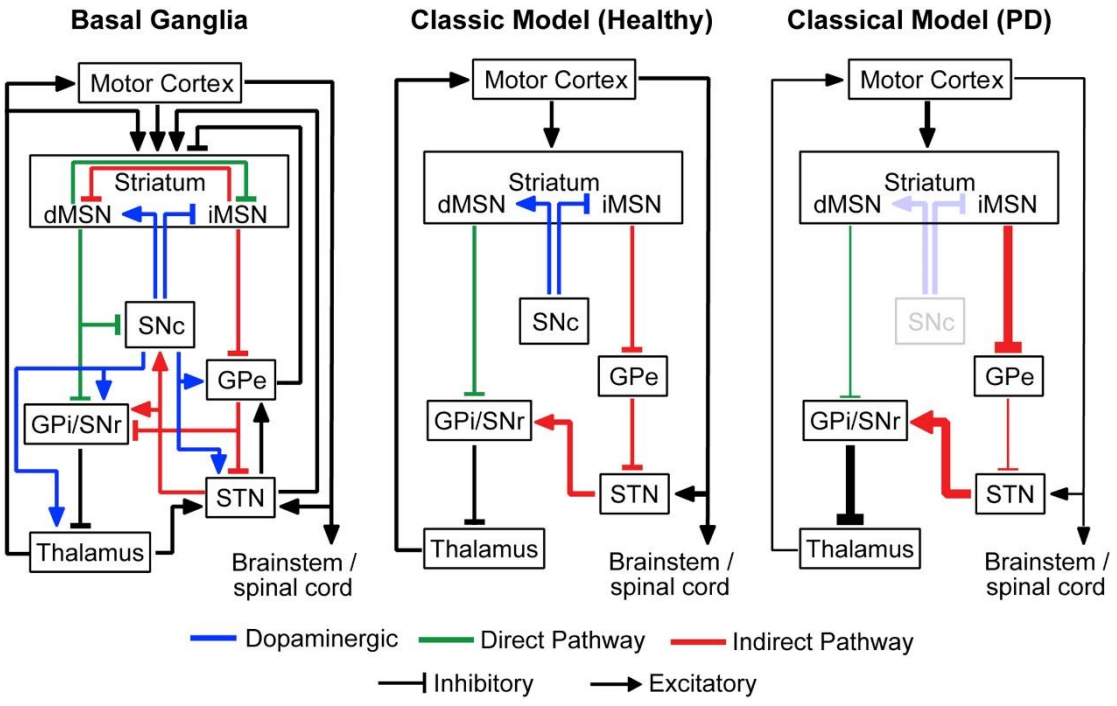

Figure 3: Classical model of basal ganglia in PD [31]
Detailed connectivity (left) and simplified model (middle and right). Indirect pathway surpasses direct pathway after dopamine depletion.

doi:10.6342/NTU202400853

1.4 Neuronal model and interconnection circuitry

The action potential is the process by which neurons change their membrane potential in a rapid series of changes (hyperpolarization -> depolarization -> repolarization -> hyperpolarization) [32]. This process is controlled by the influx and efflux of sodium cation and potassium cation across the process, which is determined by the specific set of ionic channels expressed on the neuron. The ionic channels can be classified as voltage-gated, ligand-gated, and gap junction [33]. Voltage-gated ion channels open/close the gate when reaching the reverse potential (E_{Na} for sodium ionic channel and E_K for potassium ionic channel). The ligand-gated ionic channel opens the plug when the specific ligand binds to the ionic channel and closes the plug when the specific ligand detaches. The gap junction is gated by voltage (*Cx36* is weak related, while *Cx45* is strong related) and can allow ions to flow across neurons, which direction is determined by the paired connexons channel [34].

Different ionic channels can have their conductance curves controlled by the gate factors (or opening probabilities) provided by ionic channel subunits. To achieve the maximum conductance of the ionic channel, all subunits must be in the opened state. Hodgkin and Huxley use the Boltzmann distribution to fit individual ionic channel subunit openness probability [35].

The conductance curve of a voltage-gated potassium ionic channel is best fitted with four identical factors, which can be shown [35]:

$$g_K(t) = g_{K\_max} * n^4(t)$$

The voltage-gated sodium ionic channel has an additional inactivation state, which blocks

doi:10.6342/NTU202400853

ionic flow when the membrane potential V(t) reaches peak potential. The conductance curve is fitted as follows [35]:

$$g_{Na}(t) = g_{Na\_max} * m^3(t) * h(t)$$

These gate factors m, h, n are within [0, 1]. The dynamics of gate factors can be shown as follows [35]:

$$\frac{dy}{dt} = (1 - y) * \alpha - y * \beta$$

Which α stands for the opening rate of individual plug subunits, and β stands for the closing rate of unique plug subunits.

The current of potassium ionic channel can be shown as:

$$I_K(t) = g_K(t) * (V(t) - E_K) = (g_{K\_max} * n^4(t)) * (V(t) - E_K)$$

and the current of sodium ionic channel can be shown as:

$$I_{Na}(t) = g_{Na}(t) * (V(t) - E_{Na}) = (g_{Na\_max} * m^3(t) * h(t)) * (V(t) - E_{Na})$$

However, leak channel does not need a gate factor. Therefore, the conductance is always static. Thus, the leak current can be shown as [35]:

$$I_{Leak}(t) = g_{Leak} * (V(t) - E_{Leak})$$

Synaptic ionic channels like AMPA receptor (AMPAR), GABA receptor (GABAR), and NMDA receptor (NMDAR) are ligand-gated ionic channels. However, the NMDA receptor has a magnesium ion block, which is more complex to simulate. Thus, we do not incorporate it into the model. The conductance curve of AMPAR and GABAR is fitted as follows:

$$g_{syn}(t) = g_{syn\_max} * k(t)$$

doi:10.6342/NTU202400853

The gate factor dynamics of synaptic ionic channels can also be described as the same formula in voltage-gated ionic channels. Finally, the synaptic current of AMPAR and GABAR can be shown as:

$$I_{syn}(t) = g_{syn}(t) * (V(t) - E_{syn}) = (g_{syn\_max} * k(t)) * (V(t) - E_{syn})$$

Finally, the neuronal membrane has membrane capacitance (C_m), contributing additional charging/discharging current. Kirchhoff Circuit Laws imply that the net current flow in neurons must be 0. Thus, the formula can be shown as:

$$-C_m * \frac{dv}{dt} = I_{ext} - I_{int} = (I_{inj} + I_{syn}) - (I_{Na} + I_K + I_{Leak})$$

I_{inj} is the injection current, I_{int} is the internal current, and I_{ext} is the external current.

doi:10.6342/NTU202400853

Chapter 2 Methodology

2.1 Implementation of neuronal model and interconnection Circuitry

CBT loop consists of two smaller sub-loops: the thalamocortical loop and the basal ganglia loop. Ching et al. [23] have built a single-compartment conductance-based HH thalamocortical model simulating wake and anesthesia states. The thalamocortical model consists of two brain areas and involves five neuronal types: PY, cFS, LTS, TC, and RE. Yu et al. [36] have built a single-compartment conductance-based HH basal ganglia model that simulates baseline healthy and PD states by adjusting synaptic weight. The basal ganglia model consists of four (five with TC) brain areas and involves six (seven with TC) neuronal types: dMSN, iMSN, sFS, GPe, SNr/GPi, and STN. Sasi et al. [37] introduce retinal signal to the lateral geniculate nucleus (LGN) to drive the thalamocortical loop to express steady state visually evoked potential (SSVEP). Static injection current is chosen randomly from Gaussian distribution to avoid homogeneity issues. PY also introduced additional low-amplitude randomized 10 Hz Poisson spike train as noise. Detailed CBT loop model parameters are listed in **Table 1**. Each nucleus comprises 10 neurons for the model structure, while PY consists of 40 neurons. Complex synaptic connectivity is illustrated in **Figure 4** and described in **Table 2**.

2.2 Recode previous work

The model that simulates PD firing patterns in GPe, GPi, STN, and TC in PD

doi:10.6342/NTU202400853

conditions has been implemented in our group previously [38]. We first recode this work from the Python NumPy array-based style into the Python class-based style, which has higher expandability and readability. After recoding, we further expand the striatum into the model described as [36].

2.3 Synaptic weight fitting for thalamocortical-striatal connection

TC and PY are the main striatum (dMSN, iMSN, and sFS) presynaptic neurons. Therefore, we first replace the static injection current of striatum neurons with the synaptic current provided by TC and PY. The delay range of inputs is finetuned first to mimic static current. We then finetuned the synaptic weight to reach the desired baseline striatal firing frequency range, with cFS set to 5 Hz and dMSN/iMSN set to 2 Hz [39, Fig. 3b].

doi:10.6342/NTU202400853

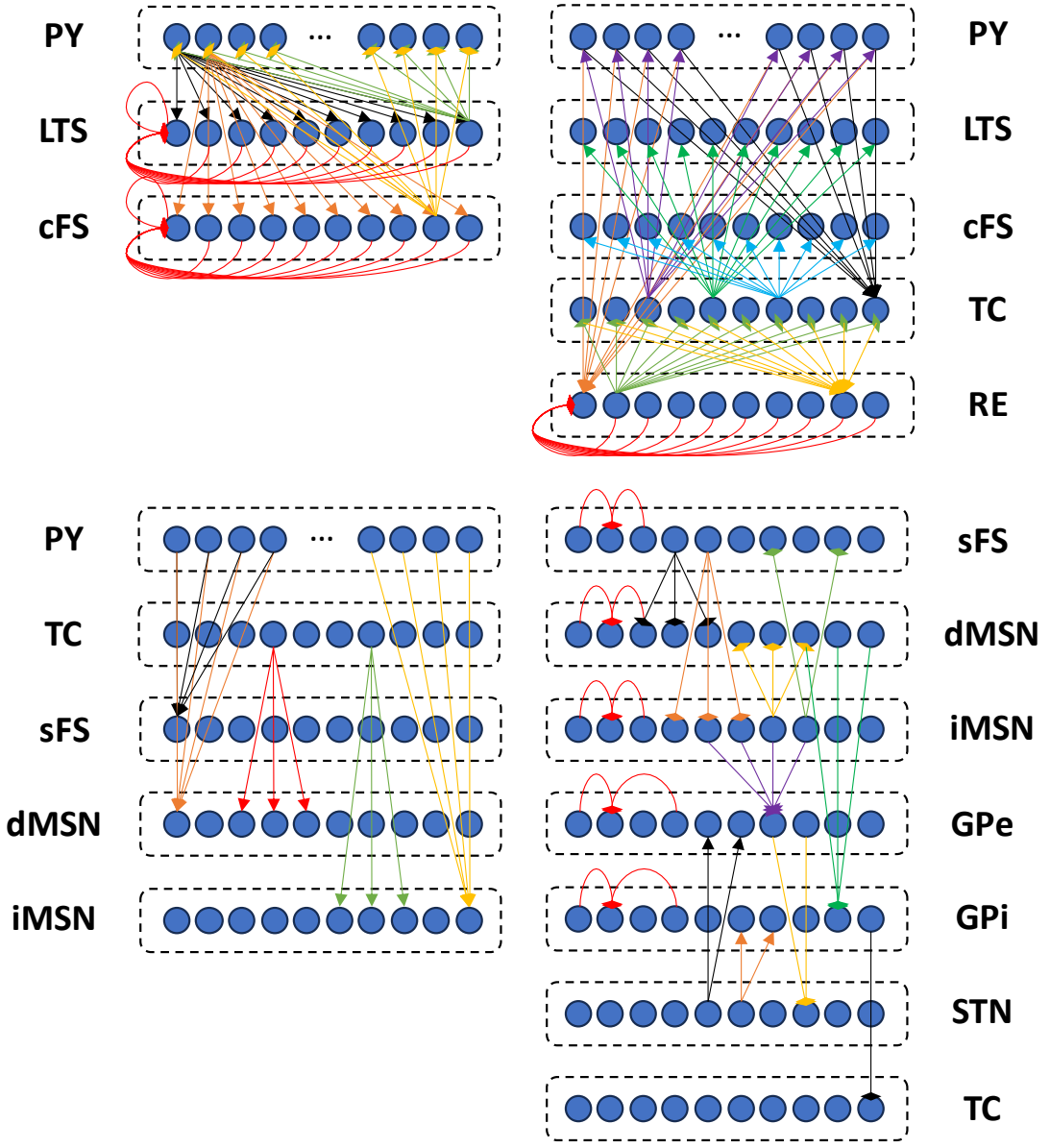

Figure 4: Synaptic connection within the model
The model has two independent cortical regions (PY, LTS, and cFS) that share the same thalamus (TC and RE).
(upper left): cortical interconnection; (upper right): thalamic interconnection and thalamocortical connection; (lower left): PY/TC to striatum connection; (lower right): basal ganglia interconnection

doi:10.6342/NTU202400853

Table 1: HH model formula

AMPAR (PY, TC, RET) gating variables:

$$\frac{dR}{dt} = (5 * (1 + \tanh(\frac{V}{4})) * (1 - R) - 0.5 * R$$

GABAR (LTS, cFS, RE) gating variables:

$$\frac{dR}{dt} = (2 * (1 + \tanh(\frac{V}{4})) * (1 - R) - 0.2 * R$$

GABAR (sFS, dMSN, iMSN, GPe) gating variables:

$$\frac{dR}{dt} = (2 * \frac{1}{1 + e^{-\frac{V+37}{2}}}) * (1 - R) - 0.04 * R$$

STN AMPAR and GPi GABAR gating variables:

$$\text{GPi: } u(t) = \begin{cases} \frac{\frac{0.3}{5*exp(-1)}}{dt}, & V(t-dt) < -10 \cap V(t) > -10 \\ 0, & V(t-dt) \geq -10 \cup V(t) \leq -10 \end{cases}$$

$$\text{STN: } u(t) = \begin{cases} \frac{\frac{0.43}{5*exp(-1)}}{dt}, & V(t-dt) < -10 \cap V(t) > -10 \\ 0, & V(t-dt) \geq -10 \cup V(t) \leq -10 \end{cases}$$

$$\frac{dZ}{dt} = u - 0.4 * Z - 0.04 * R$$

$$\frac{dR}{dt} = Z$$

For α_x and β_x:

$$\frac{dx}{dt} = \alpha_x * (1 - x) - \beta_x * x$$

For x_∞ and τ_x:

$$\frac{dx}{dt} = \frac{x_\infty - x}{\tau_x}$$

$$\text{PY: } C_m \frac{dV}{dt} = I_{app} - I_{Na} - I_K - I_{Leak} - I_M,\ I_{app} = N(1.8, 0.1)$$

$$\text{LTS: } C_m \frac{dV}{dt} = I_{app} - I_{Na} - I_K - I_{Leak} - I_M,\ I_{app} = N(1.0, 0.1)$$

$$\text{cFS: } C_m \frac{dV}{dt} = I_{app} - I_{Na} - I_K - I_{Leak},\ I_{app} = N(0.55, 0.1)$$

$$\alpha_{mNa}(V) = \frac{0.32 * -(V + 54)}{e^{-\frac{V+54}{4}} - 1}$$

$$\beta_{mNa}(V) = \frac{0.28 * (V + 27)}{e^{\frac{V+27}{5}} - 1}$$

doi:10.6342/NTU202400853

$\alpha_{hNa}(V) = 0.128 * e^{-\frac{V+50}{18}}$
$\beta_{hNa}(V) = \frac{4}{1 + e^{-\frac{V+27}{5}}}$
$\alpha_{nK}(V) = \frac{0.032 * -(V+52)}{e^{-\frac{V+52}{5}} - 1}$
$\beta_{nK}(V) = 0.5 * e^{-\frac{V+57}{40}}$
$\alpha_{mK}(V) = \frac{0.0003209 * -(V+30)}{e^{-\frac{V+30}{9}} - 1}$
$\beta_{mK}(V) = \frac{0.0003209 * (V+30)}{e^{\frac{V+30}{9}} - 1}$
$I_{Na}(V, mNa, hNa) = 50 * mNa^3 * hNa * (V - 100)$
$I_K(V, nK) = 80 * nK^4 * (V + 100)$
$I_{Leak}(V) = 0.1 * (V + 61)$
$I_M(V, mK) = 2 * mK * (V + 100)$

TC: $C_m \frac{dV}{dt} = I_{app} - I_{Na} - I_K - I_{Leak} - I_T - I_h,\ I_{app} = 0$
$\alpha_{mNa}(V) = \frac{0.32 * -(V+22)}{e^{-\frac{V+22}{4}} - 1}$
$\beta_{mNa}(V) = \frac{0.28 * (V-5)}{e^{\frac{V-5}{5}} - 1}$

doi:10.6342/NTU202400853

$\alpha_{hNa}(V) = 0.128 * e^{-\frac{V-2}{18}}$
$\beta_{hNa}(V) = \frac{4}{1 + e^{-\frac{V-5}{5}}}$
$\alpha_{nK}(V) = \frac{0.032 * -(V+10)}{e^{-\frac{V+10}{5}} - 1}$
$\beta_{nK}(V) = 0.5 * e^{-\frac{V+15}{40}}$
$mCaT_{\infty}(V) = \frac{1}{1 + e^{-\frac{V+59}{6.2}}}$
$hCaT_{\infty}(V) = \frac{1}{1 + e^{\frac{V+83}{4}}}$
$\tau_{hCaT}(V) = \frac{30.8 + \frac{211.4 + e^{\frac{V+115.2}{5}}}{1 + e^{\frac{V+86}{3.2}}}}{3.73}$
$hF_{\infty}(V) = hS_{\infty}(V) = \frac{1}{1 + e^{\frac{V+68.9}{6.5}}}$
$\tau_{hF}(V) = e^{\frac{V+183.6}{15.24}}$
$\tau_{hS}(V) = \frac{e^{\frac{V+158.6}{11.2}}}{e^{\frac{V+75}{5.5}}}$
$I_{Na}(V, mNa, hNa) = 90 * mNa^3 * hNa * (V - 50)$
$I_K(V, nK) = 80 * nK^4 * (V + 100)$
$I_{Leak}(V) = 0.01 * (V + 70) + 0.0172 * (V + 100)$
$I_{CaT}(V, hCaT) = 2 * mCaT_{\infty}(V)^2 * hCaT * (V - 120)$
$I_H(V, hF, hS) = 0.25 * hF * hS * (V + 40)$

RE: $C_m \frac{dV}{dt} = I_{app} - I_{Na} - I_K - I_{Leak} - I_T,\ I_{app} = 0$
$\alpha_{mNa}(V) = \frac{0.32 * -(V+42)}{e^{-\frac{V+42}{4}} - 1}$

doi:10.6342/NTU202400853

$\beta_{mNa}(V) = \frac{0.28 * (V + 15)}{e^{\frac{V+15}{5}} - 1}$
$\alpha_{hNa}(V) = 0.128 * e^{-\frac{V+38}{18}}$
$\beta_{hNa}(V) = \frac{4}{1 + e^{-\frac{V+15}{5}}}$
$\alpha_{nK}(V) = \frac{0.032 * -(V + 40)}{e^{-\frac{V+40}{5}} - 1}$
$\beta_{nK}(V) = 0.5 * e^{-\frac{V+45}{40}}$
$mCaT_{\infty}(V) = \frac{1}{1 + e^{-\frac{V+54}{7.4}}}$
$\tau_{mCaT}(V) = 0.44 + \frac{0.15}{e^{\frac{V+29}{10}} + e^{-\frac{V+104}{15}}}$
$hCaT_{\infty}(V) = \frac{1}{1 + e^{\frac{V+82}{5}}}$
$\tau_{hCaT}(V) = 22.7 + \frac{0.27}{e^{\frac{V+50}{4}} + e^{-\frac{V+409}{50}}}$
$I_{Na}(V, mNa, hNa) = 200 * mNa^3 * hNa * (V - 50)$
$I_K(V, nK) = 20 * nK^4 * (V + 100)$
$I_{Leak}(V) = 0.05 * (V + 90)$
$I_{CaT}(V, mCaT, hCaT) = 3 * mCaT^2 * hCaT * (V - 120)$

sFS: $C_m \frac{dV}{dt} = I_{app} - I_{Na} - I_K - I_{Leak} - I_D - I_{gap},\ I_{app} = 0$
$mNa_{\infty}(V) = \frac{1}{1 + e^{-\frac{V+24}{11.5}}}$
$hNa_{\infty}(V) = \frac{1}{1 + e^{-\frac{V+58.3}{6.7}}}$
$\tau_{hNa}(V) = 0.5 + \frac{14}{1 + e^{\frac{V+60}{12}}}$

doi:10.6342/NTU202400853

$$nK_{\infty}(V) = \frac{1}{1 + e^{-\frac{V+12.4}{6.8}}}$$
$$\tau_{nK}(V) = \left(0.087 + \frac{11.4}{1 + e^{\frac{V+14.6}{8.6}}}\right) * \left(0.087 + \frac{11.4}{1 + e^{-\frac{V-1.3}{18.7}}}\right)$$
$$mD_{\infty}(V) = \frac{1}{1 + e^{-\frac{V+50}{20}}}$$
$$hD_{\infty}(V) = \frac{1}{1 + e^{\frac{V+70}{6}}}$$
$$\tau_{mD} = 2$$
$$\tau_{hD} = 150$$
$$I_{Na}(V, hNa) = 112.5 * mNa_{\infty}(V)^3 * hNa * (V - 50)$$
$$I_K(V, nK) = 225 * nK^2 * (V + 90)$$
$$I_{Leak}(V) = 0.1 * (V + 70)$$
$$I_D(V, mD, hD) = 6 * mD^3 * hD * (V + 90)$$
$$I_{gap}(V) = 0.1 * (V - V_{presynaptic})$$

dMSN/iMSN: $C_m \frac{dV}{dt} = I_{app} - I_{Na} - I_K - I_{Leak} - I_M - I_{CaL} - I_{Kir},\ I_{app} = 0$
$$\alpha_{mNa}(V) = \frac{0.32 * -(V + 54)}{e^{-\frac{V+54}{4}} - 1}$$
$$\beta_{mNa}(V) = \frac{0.28 * (V + 27)}{e^{\frac{V+27}{5}} - 1}$$
$$\alpha_{hNa}(V) = 0.128 * e^{-\frac{V+50}{18}}$$
$$\beta_{hNa}(V) = \frac{4}{1 + e^{-\frac{V+27}{5}}}$$
$$\alpha_{nK}(V) = \frac{0.032 * -(V + 52)}{e^{-\frac{V+52}{5}} - 1}$$
$$\beta_{nK}(V) = 0.5 * e^{-\frac{V+57}{40}}$$

doi:10.6342/NTU202400853

$\alpha_{mk}(V) = \frac{0.0003209 * -(V+30)}{e^{-\frac{V+30}{9}} - 1}$
$\beta_{mk}(V) = \frac{0.0003209 * (V+30)}{e^{\frac{V+30}{9}} - 1}$
$mCaL_{\infty}(V) = \frac{1}{1 + e^{-\frac{V+33}{6.7}}}$
$hCaL_{\infty}(V) = \frac{1}{1 + e^{-\frac{V+13.4}{11.9}}}$
$\tau_{mCaL}(V) = \frac{1}{0.1194 * \frac{V+8.124}{e^{\frac{V+8.124}{9.005}} - 1} + 2.97 * e^{\frac{V}{31.4}}}$
$\tau_{hCaL} = 14.77$
$I_{Na}(V, mNa, hNa) = 100 * mNa^3 * hNa * (V - 50)$
$I_K(V, nK) = 80 * nK^4 * (V + 100)$
$I_{Leak}(V) = 0.1 * (V + 67)$
$I_M(V, mk) = 2 * mk * (V + 100)$
$I_{CaL}(V, mCaL, hCaL) = (0.000000425 * mCaL^2 * hCaL) * \frac{(2 * 96489 * 74.87 * V^2) * (0.002 - 0.000006 * e^{-74.87*V})}{1 - e^{-74.87*V}}$
$I_{Kir}(V) = g_{Kir} * \frac{V+82}{1 + e^{\frac{V+102}{13}}}$ $g_{Kir} = 0.175$ if dMSN; $g_{Kir} = 0.14$ if iMSN

GPe /GPi: $C_m \frac{dV}{dt} = I_{app} - I_{Na} - I_K - I_{Leak} - I_{CaT} - I_{CaL} - I_{AHP}$, $I_{app\_GPe} = N(21, 0.1)$, $I_{app\_GPi} = N(22, 0.1)$
$mNa_{\infty}(V) = \frac{1}{1 + e^{-\frac{V+37}{10}}}$
$hNa_{\infty}(V) = \frac{1}{1 + e^{\frac{V+58}{12}}}$

doi:10.6342/NTU202400853

$$nK_{\infty}(V) = \frac{1}{1 + e^{-\frac{V+50}{14}}}$$
$$aCaT_{\infty}(V) = \frac{1}{1 + e^{-\frac{V+57}{2}}}$$
$$rCaT_{\infty}(V) = \frac{1}{1 + e^{\frac{V+70}{2}}}$$
$$cCaL_{\infty}(V) = \frac{1}{1 + e^{-\frac{V+35}{2}}}$$
$$\tau_{hNa}(V) = \tau_{nK}(V) = 0.05 + \frac{0.27}{1 + e^{\frac{V+40}{12}}}$$
$$\tau_{rCaT} = 30$$
$$\frac{dhNa}{dt} = 0.05 * \frac{hNa_{\infty}(V) - hNa}{\tau_{hNa}(V)}$$
$$\frac{dnK}{dt} = 0.1 * \frac{nK_{\infty}(V) - nK}{\tau_{nK}(V)}$$
$$\frac{drCaT}{dt} = \frac{rCaT_{\infty}(V) - rCaT}{\tau_{rCaT}}$$
$$\frac{dCa}{dt} = 0.0001 * (-I_{CaT}(V, rCaT) - I_{CaL}(V) - 15 * Ca)$$
$$I_{Na}(V, mNa, hNa) = 120 * mNa_{\infty}(V)^3 * hNa * (V - 55)$$
$$I_K(V, nK) = 30 * nK^4 * (V + 80)$$
$$I_{Leak}(V) = 0.1 * (V + 65)$$
$$I_{CaT}(V, rCaT) = 0.5 * aCaT_{\infty}(V)^3 * rCaT * (V - 120)$$
$$I_{CaL}(V) = 0.15 * cCaL_{\infty}(V)^2 * (V - 120)$$
$$I_{AHP}(V, Ca) = 10 * \frac{Ca}{Ca + 10} * (V + 80)$$

STN: $C_m \frac{dV}{dt} = I_{app} - I_{Na} - I_K - I_{Leak} - I_{CaT} - I_{CaL} - I_{AHP},\ I_{app} = N(33, 0.1)$
$$mNa_{\infty}(V) = \frac{1}{1 + e^{-\frac{V+30}{15}}}$$

doi:10.6342/NTU202400853

$$hNa_{\infty}(V) = \frac{1}{1 + e^{\frac{V+39}{3.1}}}$$
$$nK_{\infty}(V) = \frac{1}{1 + e^{-\frac{V+32}{8}}}$$
$$aCaT_{\infty}(V) = \frac{1}{1 + e^{-\frac{V+63}{7.8}}}$$
$$bCaT_{\infty}(r) = \frac{1}{1 + e^{-\frac{r-0.4}{0.1}}} - \frac{1}{1 + e^{4}}$$
$$rCaT_{\infty}(V) = \frac{1}{1 + e^{\frac{V+67}{2}}}$$
$$cCaL_{\infty}(V) = \frac{1}{1 + e^{-\frac{V+20}{8}}}$$
$$\tau_{hNa}(V) = 1 + \frac{500}{1 + e^{\frac{V+57}{3}}}$$
$$\tau_{nK}(V) = 1 + \frac{100}{1 + e^{\frac{V+80}{26}}}$$
$$\tau_{rCaT}(V) = 7.1 + \frac{17.5}{1 + e^{\frac{V+68}{2.2}}}$$
$$\tau_{cCaL}(V) = 1 + \frac{10}{1 + e^{\frac{V+80}{26}}}$$
$$\frac{dhNa}{dt} = 0.75 * \frac{hNa_{\infty}(V) - hNa}{\tau_{hNa}(V)}$$
$$\frac{dnK}{dt} = 0.75 * \frac{nK_{\infty}(V) - nK}{\tau_{nK}(V)}$$
$$\frac{drCaT}{dt} = 0.2 * \frac{rCaT_{\infty}(V) - rCaT}{\tau_{rCaT}(V)}$$
$$\frac{dcCaL}{dt} = 0.08 * \frac{cCaL_{\infty}(V) - cCaL}{\tau_{cCaL}(V)}$$
$$\frac{dCa}{dt} = 0.0000375 * (-I_{CaT}(V, rCaT) - I_{CaL}(V) - 22.5 * Ca)$$

doi:10.6342/NTU202400853

$I_{Na}(V, mNa, hNa) = 37 * mNa_{\infty}(V)^3 * hNa * (V - 55)$
$I_K(V, nK) = 45 * nK^4 * (V + 80)$
$I_{Leak}(V) = 2.25 * (V + 60)$
$I_{CaT}(V, rCaT) = 0.5 * aCaT_{\infty}(V)^3 * bCaT_{\infty}(rCaT)^2 * (V - 140)$
$I_{CaL}(V, cCaL) = 2 * cCaL^2 * (V - 140)$
$I_{AHP}(V, Ca) = 20 * \frac{Ca}{Ca + 15} * (V + 80)$

doi:10.6342/NTU202400853

Table 2: Synaptic connection parameters

	PY	LTS	cFS	TC	RE	sFS	dMSN	iMSN	GPe	GPi	STN
PY		40 (0.01)	40 (0.04)	40*2 (0.0125)	40*2 (0.001)	4*2 (0.399)	4*2 (0.08)	4*2 (0.08)			
LTS	10 (0.032)	10 (0.015)									
cFS	10 (0.032)		10 (0.01)								
TC	10 (0.01)	10 (0.01)	10 (0.04)		10 (0.001)		3 (0.056)	3 (0.056)			
RE				10 (0.003)	9 (0.0067)						
sFS						2 (0.1)	3 (0.08)	3 (0.11)			
dMSN							2 (0.02)	2 (0.05)		3 (0.1)	
iMSN							3 (0.03)	2 (0.05)	4 (0.1)		
GPe									2 (0.5)	2 (0.5)	2 (0.5)
GPi				1 (0.003)							
STN									2 (0.15)	2 (0.15)	
RET	1 (0.01125)			1 (1.5)							

Synaptic connection per type of neuron: presynaptic connections (synaptic maximum conductance per neuron)
Row: presynaptic neuron type; Column: postsynaptic neuron type

doi:10.6342/NTU202400853

2.4 Conditions for aroused state and PD state

The simulation states combine baseline (healthy)/PD and wake/sleep (NREM)/anesthesia. When comparing PD state to baseline state, cortical-to-dMSN/iMSN maximum synaptic conductance is decreasing/rising 10%, sFS-to-dMSN/iMSN maximum synaptic conductance is dropping 30%, sFS M-type potassium channel maximum conductance is changed from 2.0 nS to 1.2 nS, as well as shifting injection current baseline of GPe, GPi and STN from 21/22/33 μA to 8/16/23 μA [40].

The wake/anesthesia state influences GABAergic neurons' synaptic conductance and refractory time constant in the CBT loop [41]. Meanwhile, the wake/sleep state affects the synaptic conductance of leak channels of neurons in the CBT loop [42], [43]. For a simple simulation of NREM EEG recordings, we revised the shape of the injection current in the sleep state from static to square wave. The frequency of square waves differs between the baseline and PD states, with the former at 2 Hz and the latter at 3 Hz (roughly estimated from [21, Fig. 2]). Summary is concluded in **Table 3**.

2.5 DBS and visual stimulation

For high-frequency DBS, 130 Hz DBS with 0.06 ms, 5 mA/cm^2 pulse is chosen. The target of DBS can be the thalamus and nucleus in the basal ganglia. Here, we select STN as the DBS site, the most common target in treating PD. For visual stimulation, although a lower-order CBT loop preprocesses the visual stimulus, it can then be propagated to a higher-order CBT loop that might receive sensual and motor information. Sasi et al. [37, Figs. 2c & 2d] shows that the firing frequency of the LGN is entrained as retinal input.

doi:10.6342/NTU202400853

Therefore, we can simplify the visual simulation with a retinal cell (RET) firing uniform 10 Hz or 40 Hz spike train, which is 0 mV at resting and 1 ms, 10 mV of firing period, to represent a lower-order TC that receives visual stimulation and is input to every PY and TC. Moreover, we hypothesized that the visual stimulation is strong enough to drive the striatum to choose. In other words, the retinal input is able to increase the firing rate of cFS from 5 Hz to 15 Hz, and dMSN/iMSN from 2 Hz to 8 Hz [39, Figs. 3b & 4b].

2.6 Model simulation

The code is written in Python 3.9, the compiler is Spyder, and the version control application is Anaconda. The integration method used in the HH model is the Newton-Raphson method. The simulation timestep is 0.01 ms, the total simulation time is 3 s, and the results are averaged from 10 simulations.

2.7 Data analysis

The first 1000 ms is discarded for the model not yet stabilized. The processed data, which includes membrane voltage and synaptic current, are used for EEG, firing pattern, and firing rate analysis. For the EEG analysis, we first averaged all postsynaptic currents of neurons in the targeted cell type. The power spectrum density (PSD) is derived from the Fourier transform of the averaged current. Before averaging the PSD as a final result, every PSD result from a single simulation is normalized by the total beta power, ranging from 13 Hz to 30 Hz. For the firing pattern analysis, we plot each neuron's firing events. The definition is the time that the neuron’s membrane voltage is at a rising period and just passed 0 mV, which is much higher than the action potential threshold voltage. These

doi:10.6342/NTU202400853

criteria avoid multiple counting of the firing event. For the firing rate analysis, the averaged firing frequency equals the summation of total firing events of neurons in the targeted cell type, then divided by the size of the targeted cell type.

doi:10.6342/NTU202400853

Table 3: State-related parameters

		Baseline, wake	**Baseline, NREM**	**Baseline, anesthesia**	**PD, wake**	**PD, NREM**	**PD, anesthesia**
Circadian rhythm [42], [43]	Injection current duty cycle and frequency	static	50%, 2 Hz	static	static	50%, 3 Hz	static
Anesthesia [23], [41]	GABAR maximal conductance factor	X1	X4		X1	X4	
	GABAR refractory rate factor	X1	X4		X1	X4	
PD [40]	Basal ganglia injection current (I_{app})	GPe: 21 GPi: 22 STN: 33			GPe: 8 GPi: 16 STN: 23		
	Striatum synaptic maximal conductance factor	X1			PY -> sFS: X0.7 PY/TC -> dMSN/iMSN: X0.95/X1.05 (weak), X0.9/X1.1 (medium), X0.85/X1.15 (strong) sFS -> dMSN/iMSN: X0.8		

doi:10.6342/NTU202400853

Chapter 3 Results

3.1 Finetune synaptic connection from thalamocortical to striatum

The striatum (dMSN, iMSN, and sFS) and TC should be connected through the synapse to concatenate the thalamocortical and basal ganglia loop. Furthermore, these connected nodes' firing patterns must reference the pattern shown in the original model or in vivo/vitro.

The Striatum neurons HH model from Yu et al. [36] is activated by static injection current. Therefore, we replace the injection currents with shifting and stacking synaptic currents from PY/TC to the striatum. **Figure 5a** shows that static injection current can be approximated by going and stacking similar synaptic inputs. Whole loop simulation in irregular firing also shows more intense peaks and lower summation current amplitude (**Figure 5b & 5c**). Though little previous research uses the shifting and stacking technique, some in silico research shows that introducing synaptic latency will affect neuronal firing patterns [44].

doi:10.6342/NTU202400853

(a)

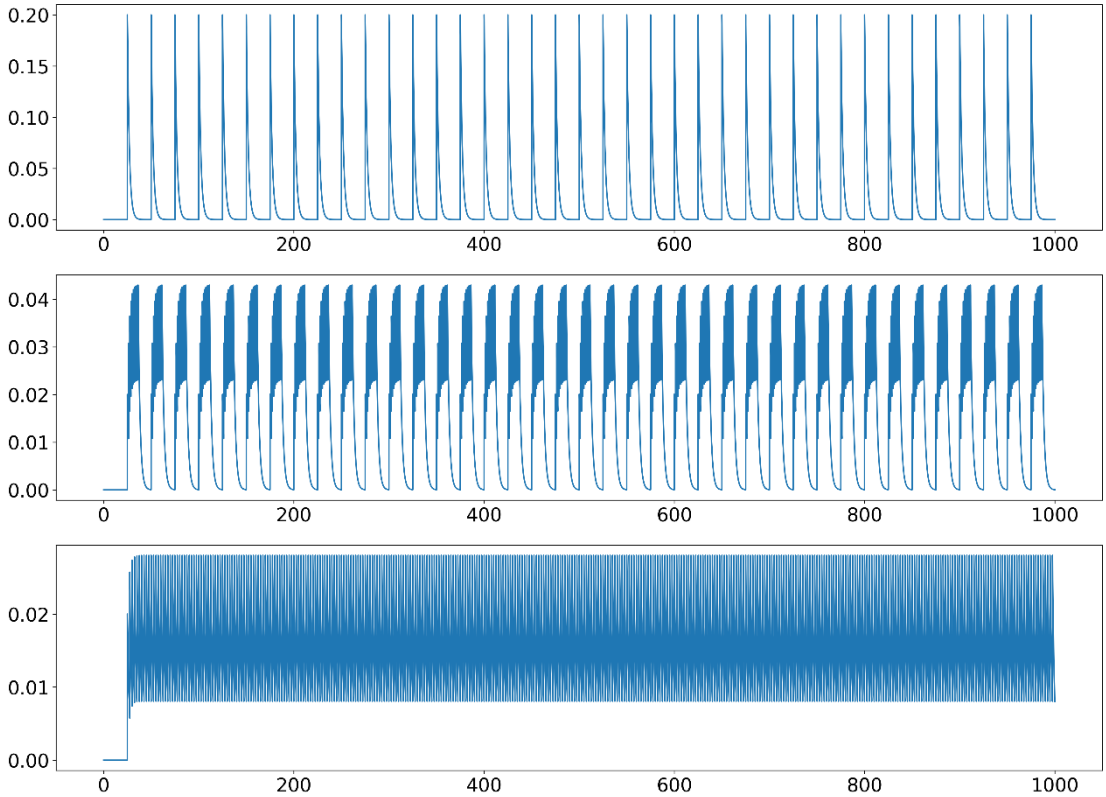

(b)

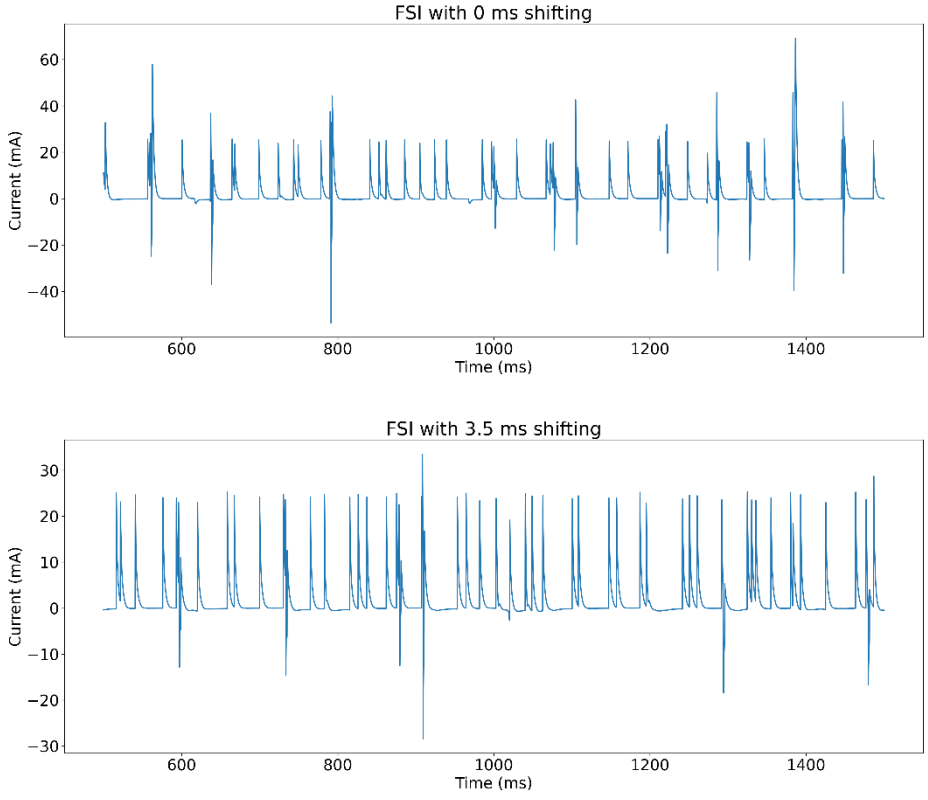

doi:10.6342/NTU202400853

(c)

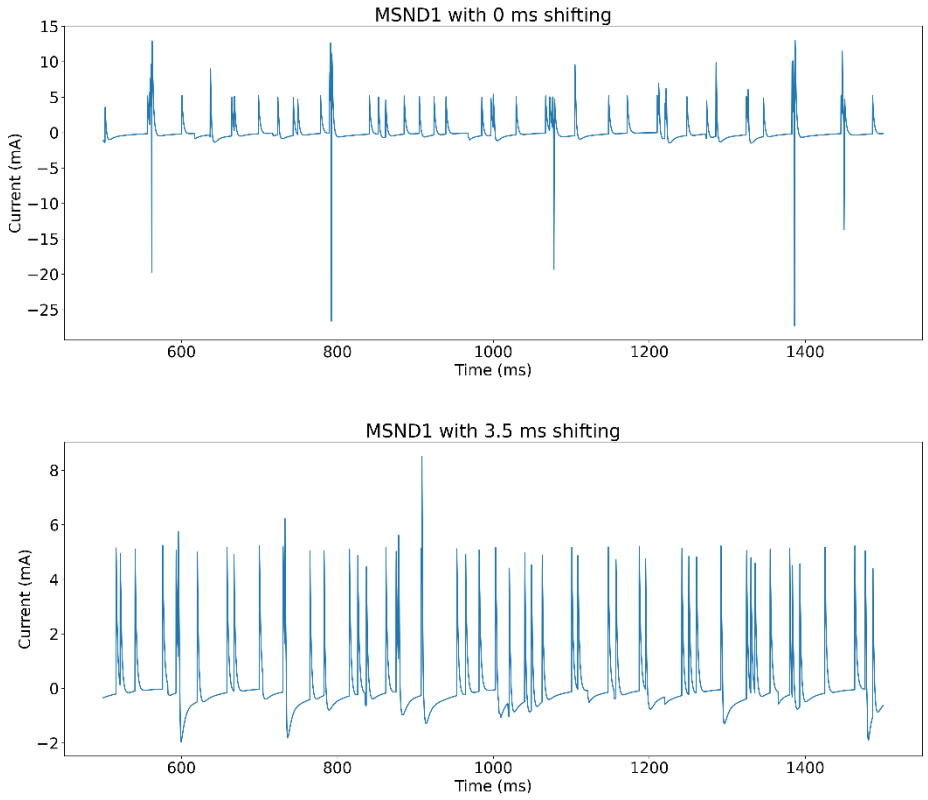

Figure 5: Shifting and stacking of synaptic input can mimic static current
(a) Original synaptic pulse: uniformly distributed 40 Hz spike train.
(Upper): stacking ten pulses that are not shifting; (middle): stacking ten pulses that are 12.5 ms uniform gradual shifting; (lower): stacking ten pulses that are 25 ms uniform gradual shifting.
(b) Synaptic current of baseline/wake FSI under different shifting condition.
(Upper): stacking pulses that are not shifting; (lower): stacking pulses that are 3.5 ms uniform gradual shifting.
(c) Synaptic current of baseline/wake dMSN under different shifting condition.
(Upper): stacking pulses that are not shifting; (lower): stacking pulses that are 3.5 ms uniform gradual shifting.

3.2 Model reproduces arousal state and progressing PD state

After model bridging, the model is run with sets of state-related parameters mentioned in **Table 3**. **Figure 6a** shows that a pathological beta wave emerges in a PD wake state. PD influences the basal ganglia loop more than the thalamocortical loop, with pathological beta power being most significant in STN (**Figure 6a**). Besides, when PD

doi:10.6342/NTU202400853

severity rises, both types of MSNs are excited due to decreased inhibition from sFS, while dMSN is less excited and iMSN is more excited (**Figure 6b**).

3.3 Visual stimulation efficacy versus STN DBS efficacy

The model is run with inputs to compare how STN DBS and visual stimulation affect PD, which is mentioned in **Table 3**. In biphasic 130 Hz STN DBS, the potentiated thalamocortical loop is depressed by STN DBS (**Figure 7a**). Pathological beta power is depressed after STN DBS as expected (**Figure 7a**). However, STN DBS does not recover most neurons firing patterns under PD (**Figure 7b**). In visual stimulation, pathological beta power in STN and TC is strongly depressed (**Figure 8b**). However, other neurons do not show significant PSD or firing frequency changes compared to PD (**Figure 8b, 8e**).

Though 10 Hz and 40 Hz visual stimulation do not show the difference in firing frequency, PSD, and regulating pathological beta power in PD (**Figure 8b, 8e**), 40 Hz visual stimulation is chosen because it has little side effects like dizziness compared to 10 Hz visual stimulation. **Figure 9a, 9b** shows that visual stimulation does not depress pathological beta power as strongly as STN DBS. Moreover, **Figure 8c, 8f** shows that the PSD and firing range of TC with 40 Hz visual stimulation is similar to that of 40 Hz visual stimulation in the baseline conditions, which indicates that visual stimulation might dilute the pathological beta wave to other connected CBT loop.

doi:10.6342/NTU202400853

(a)

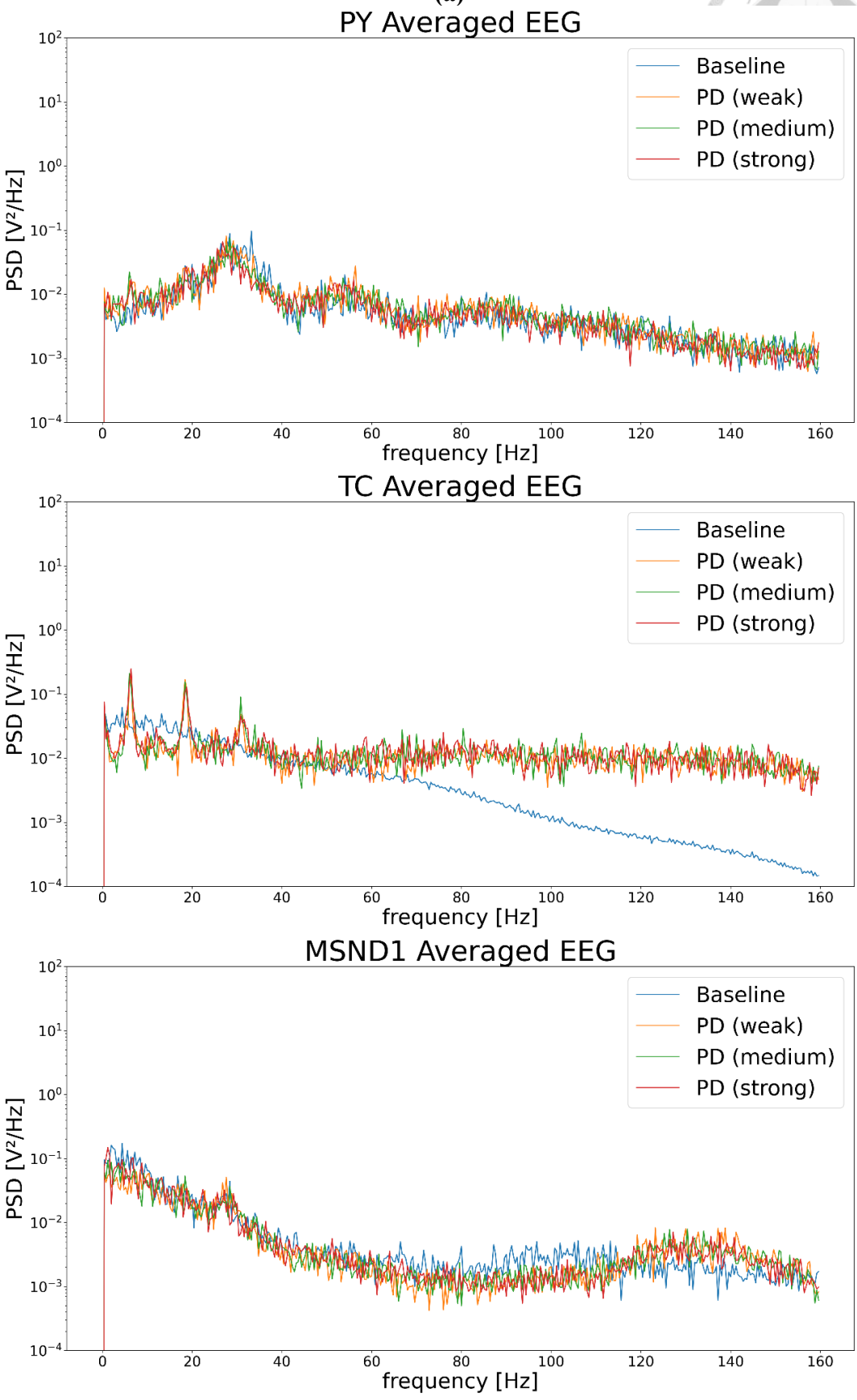

doi:10.6342/NTU202400853

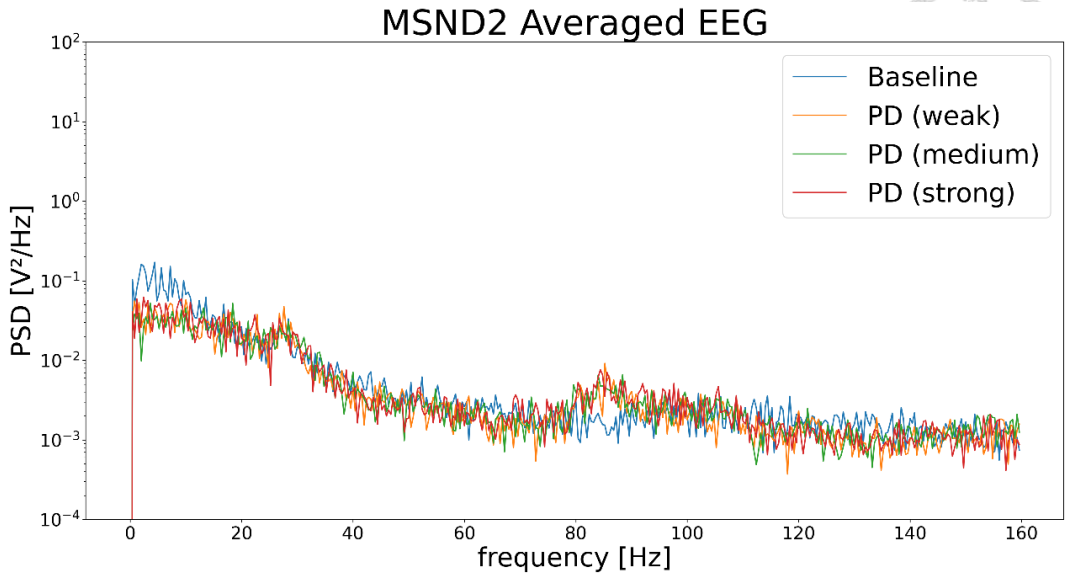

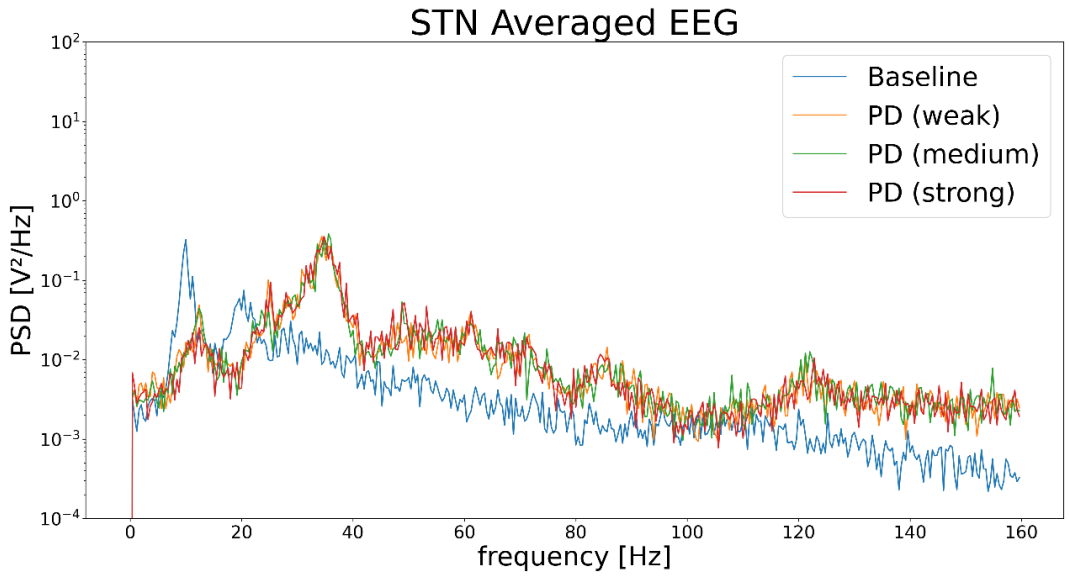

(b)

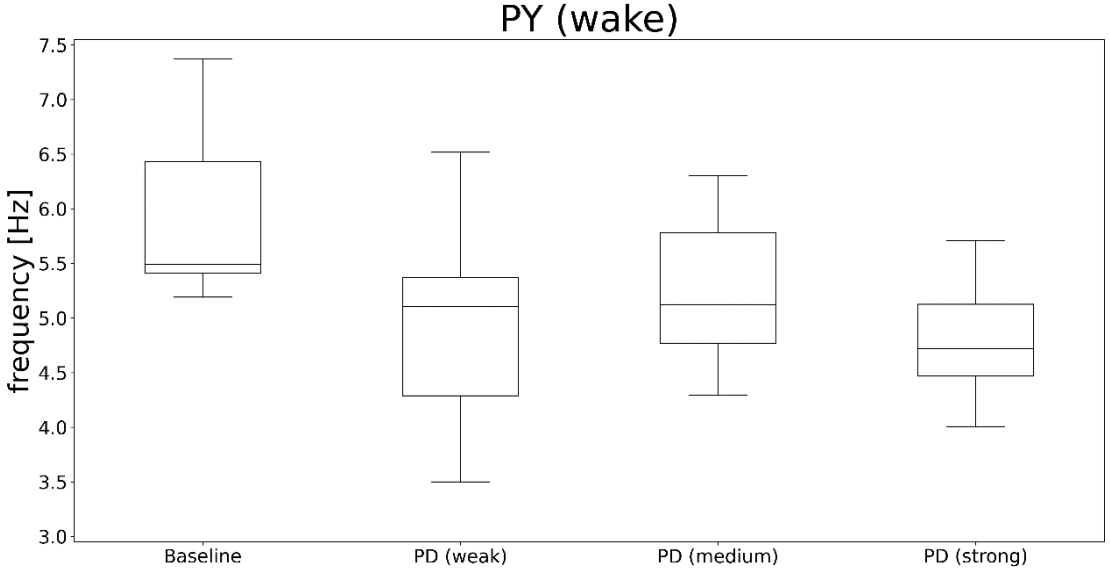

doi:10.6342/NTU202400853

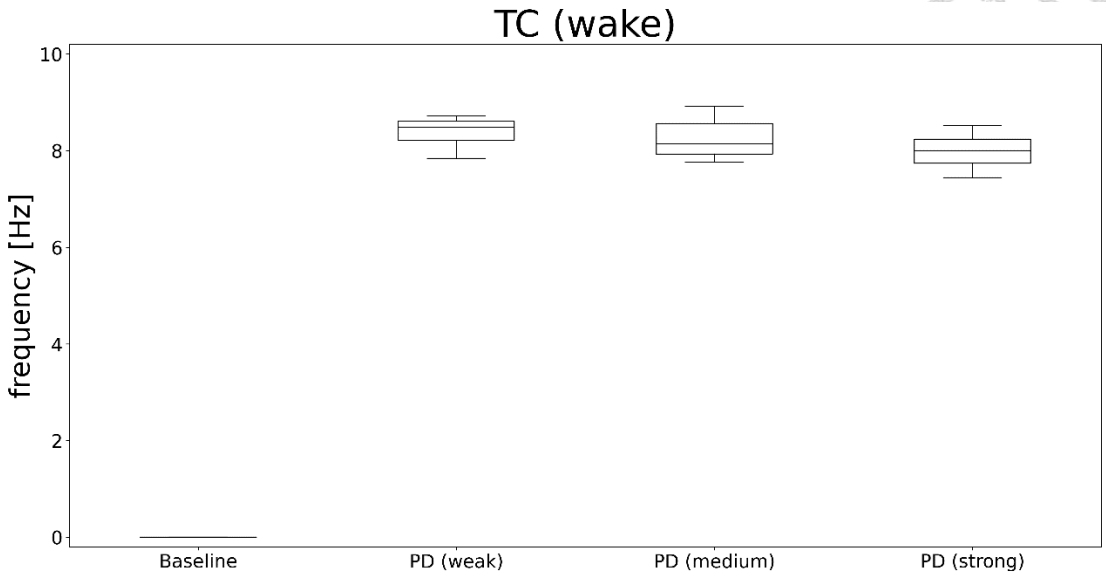

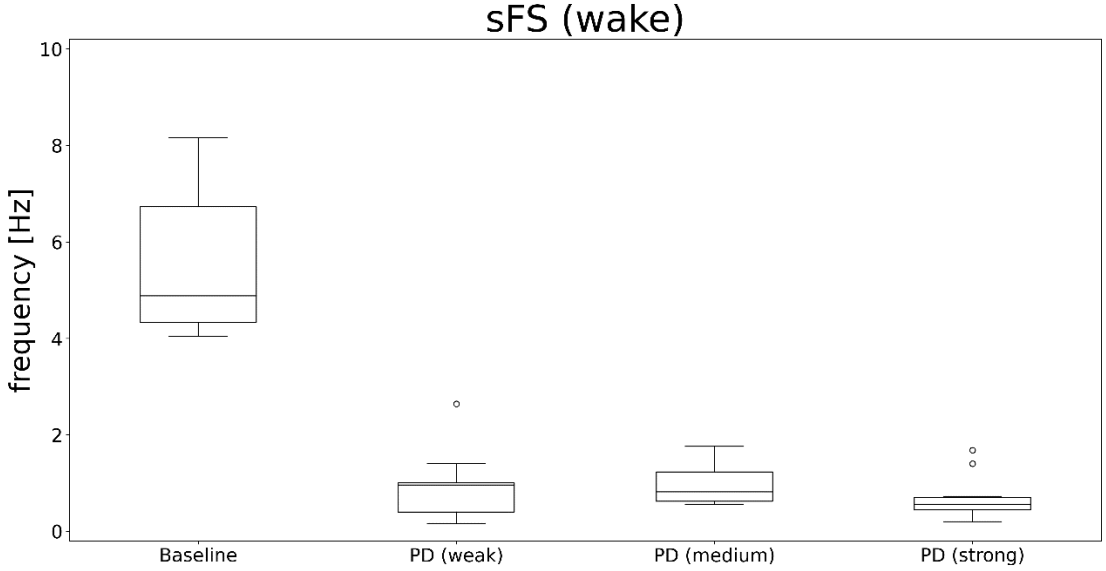

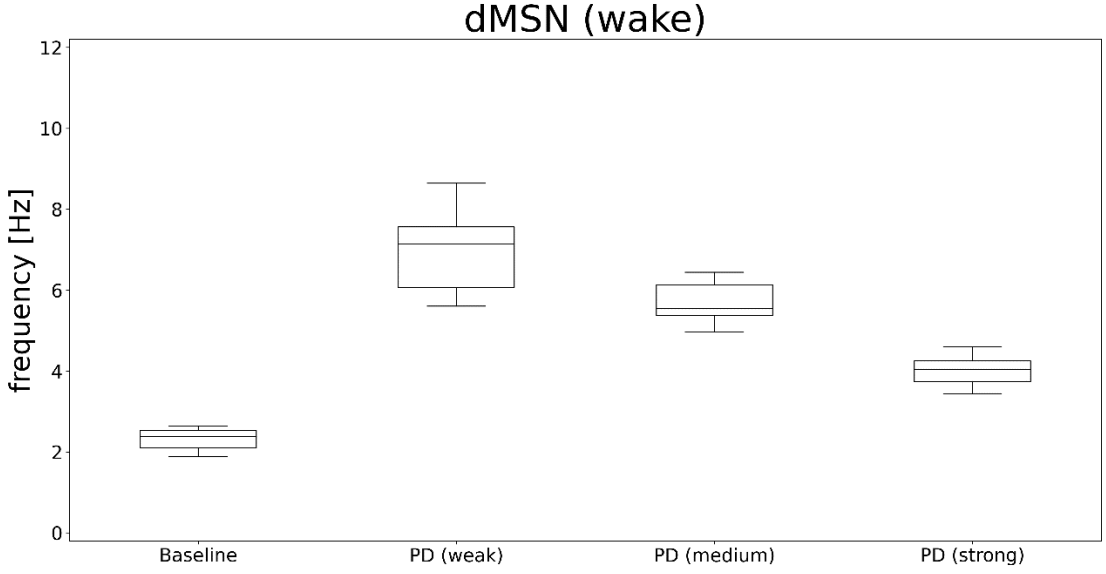

doi:10.6342/NTU202400853

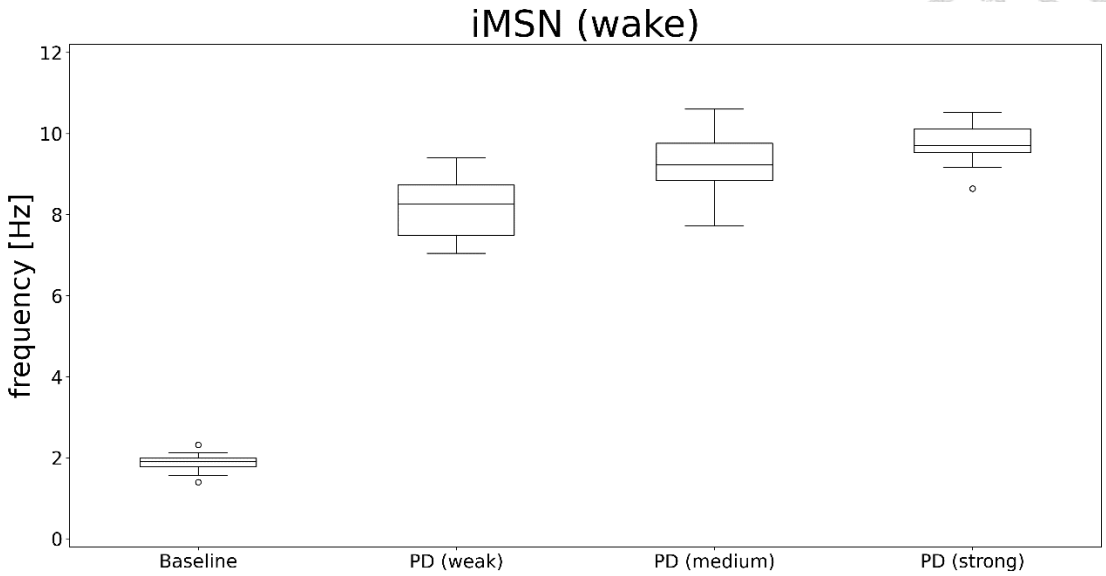

Figure 6: Model under different stages of PD

(a) PSD of neurons from top to down (PY, TC, dMSN, iMSN, STN) and from left to right (baseline, weak PD, medium PD, and strong PD). The X-axis is fixed at (0, 160), and the Y-axis is fixed at (1e-4, 1e+2).

(b) Firing frequency range of neurons from top to down (PY, TC, sFS, dMSN, iMSN) and from left to right (baseline, weak PD, medium PD, and strong PD).

doi:10.6342/NTU202400853

(a)

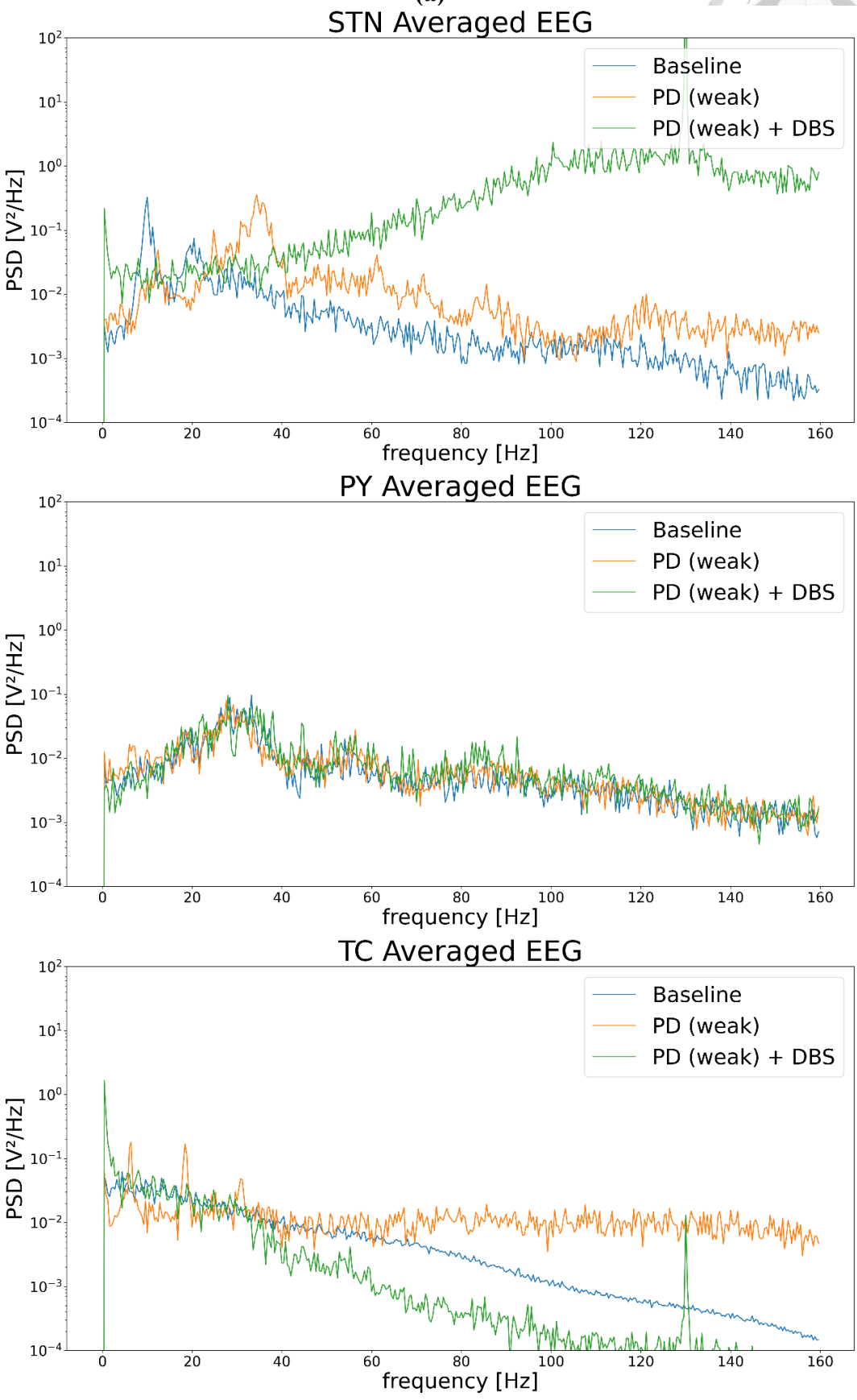

doi:10.6342/NTU202400853

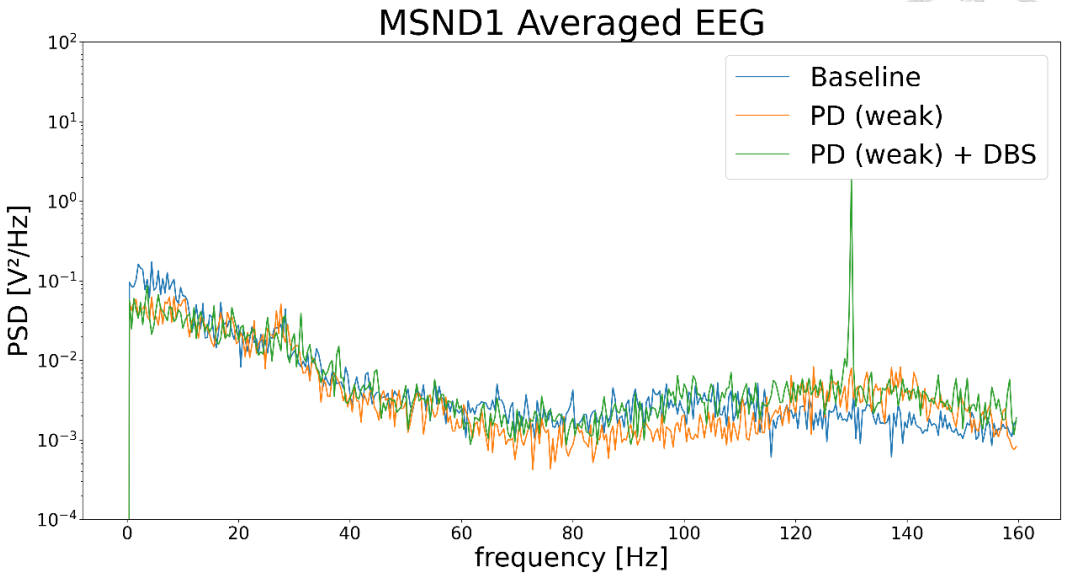

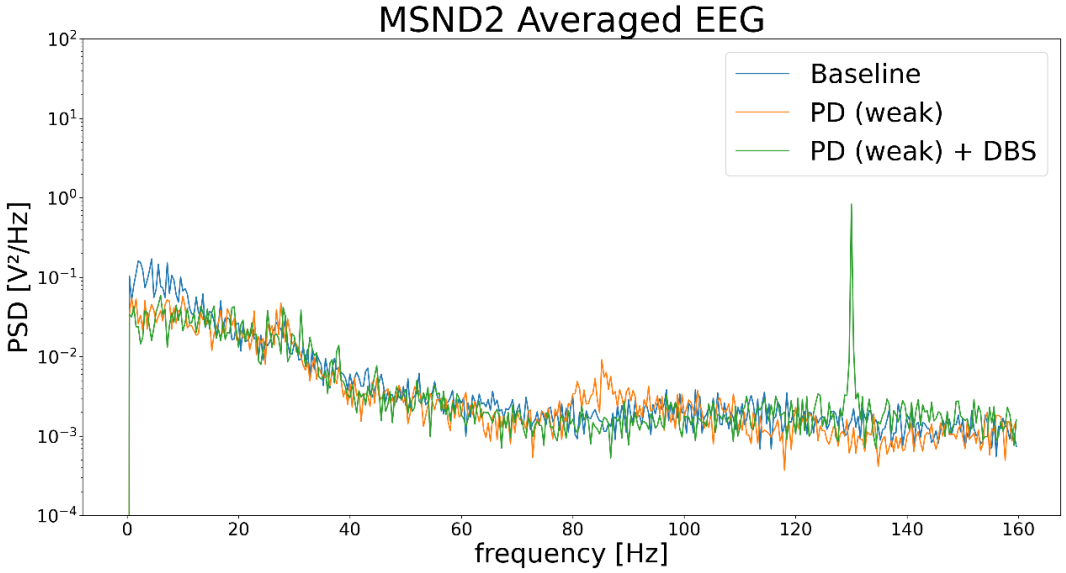

(b)

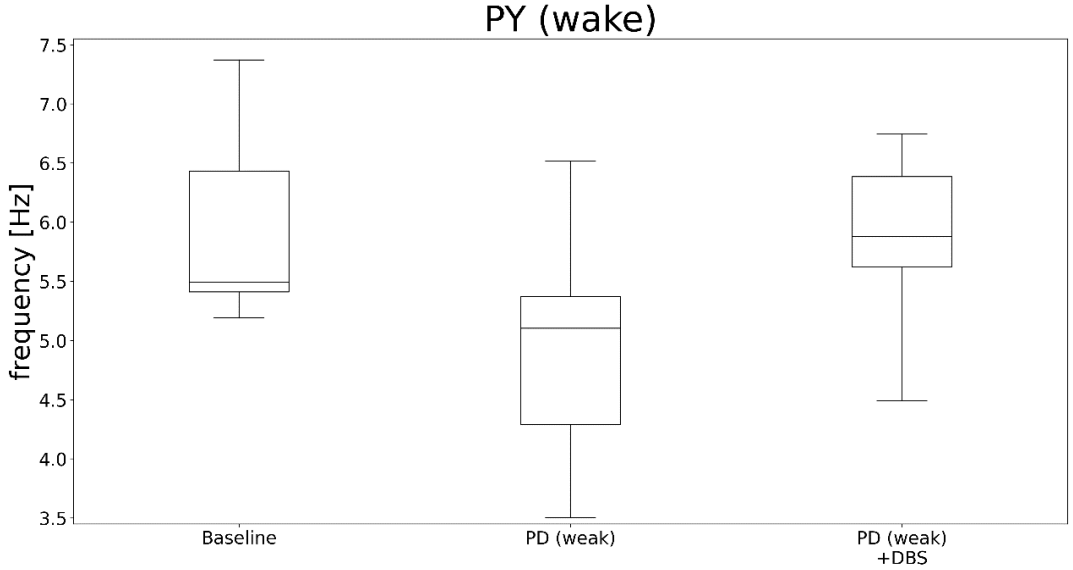

doi:10.6342/NTU202400853

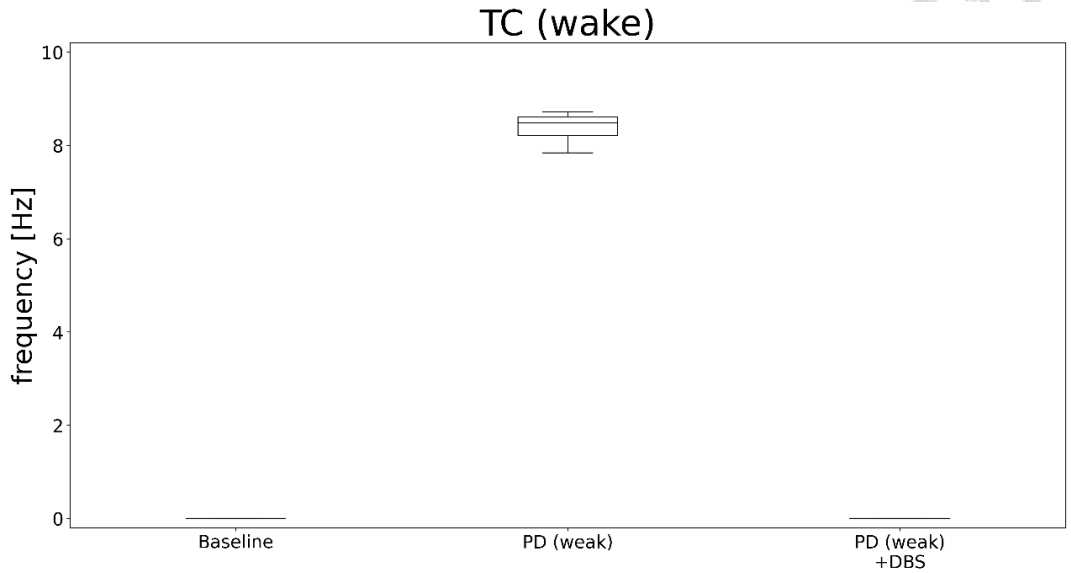

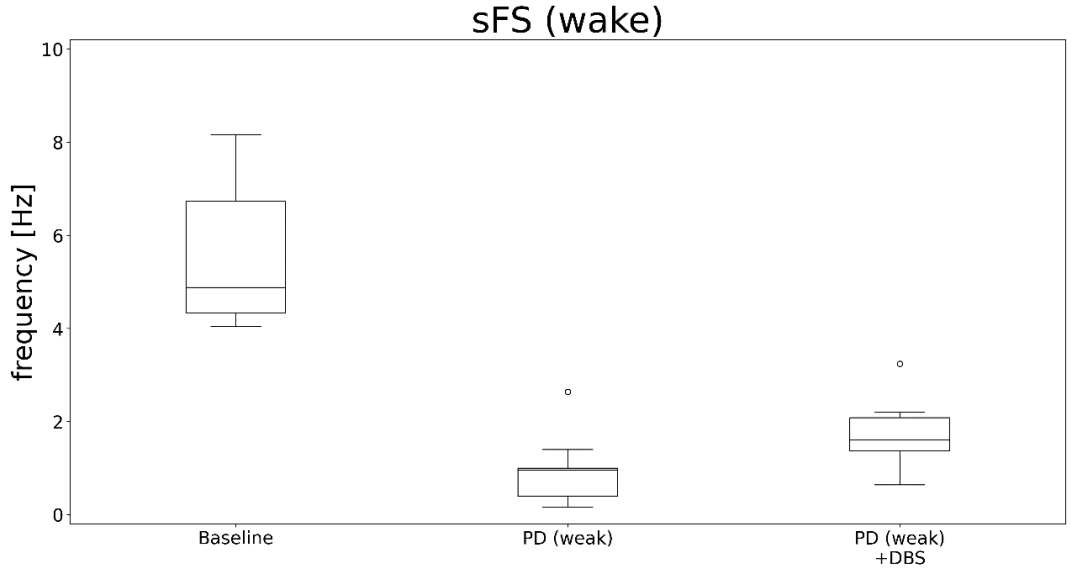

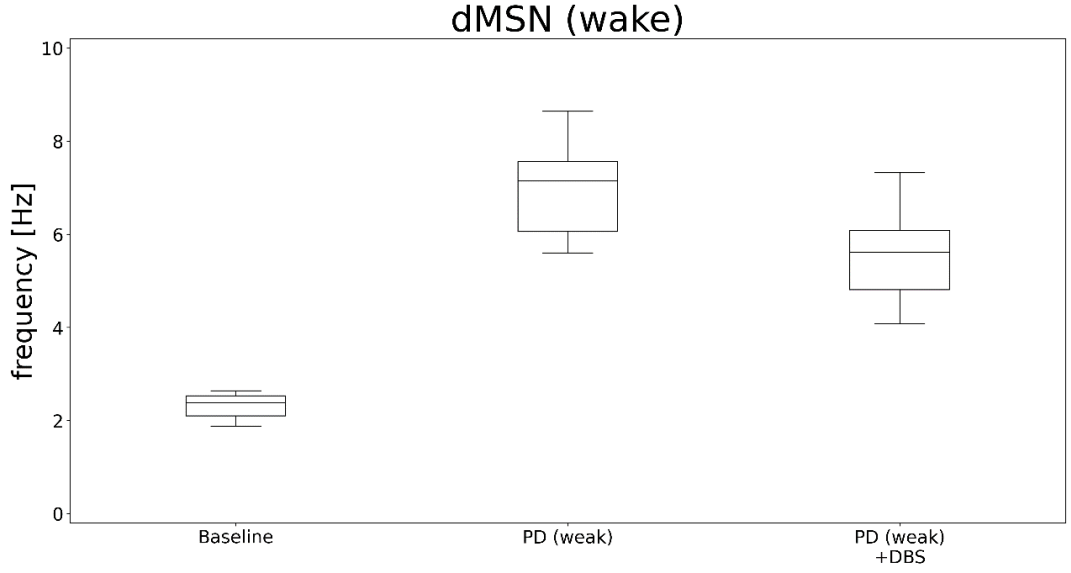

doi:10.6342/NTU202400853

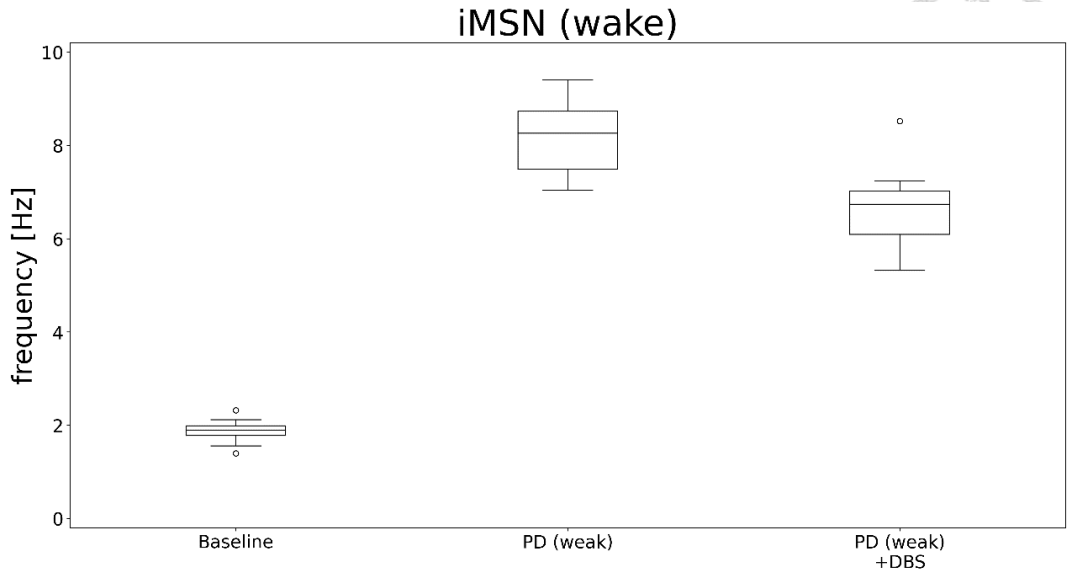

Figure 7: Model under DBS

(a) PSD of neurons from top to down (STN, PY, TC, dMSN, iMSN) and from left to right (baseline, weak PD, weak PD + DBS). The X-axis is fixed at (0, 160), and the Y-axis is fixed at (1e-4, 1e+2).

(b) Firing frequency range of neurons from top to down (PY, TC, sFS, dMSN, iMSN) and from left to right (baseline, weak PD, weak PD + DBS).

doi:10.6342/NTU202400853

(a)

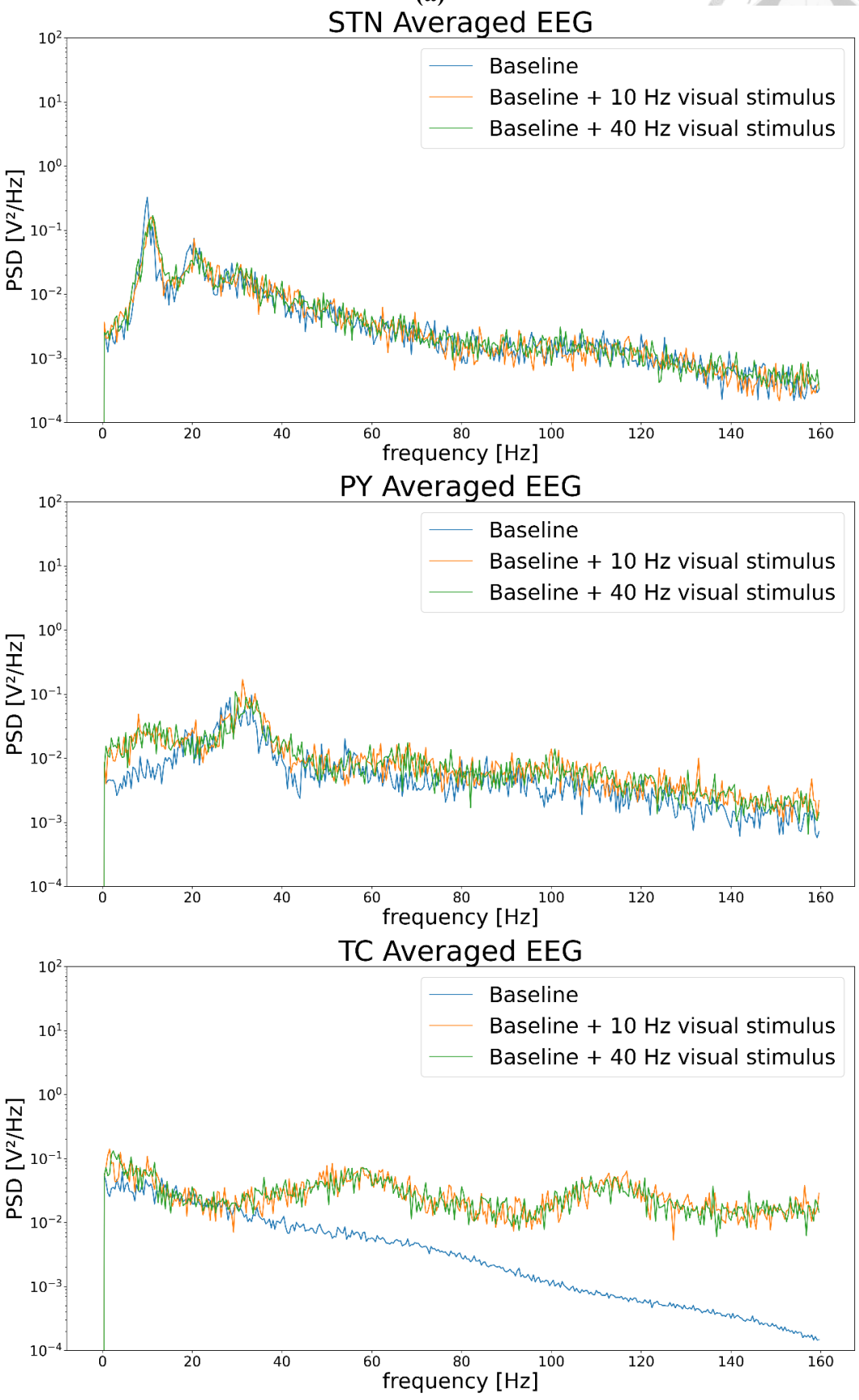

doi:10.6342/NTU202400853

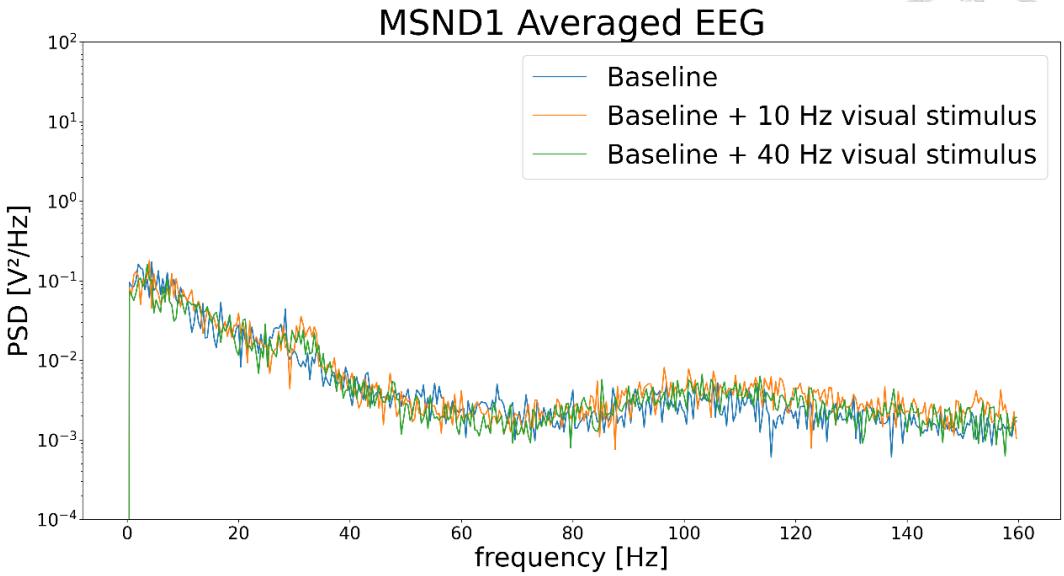

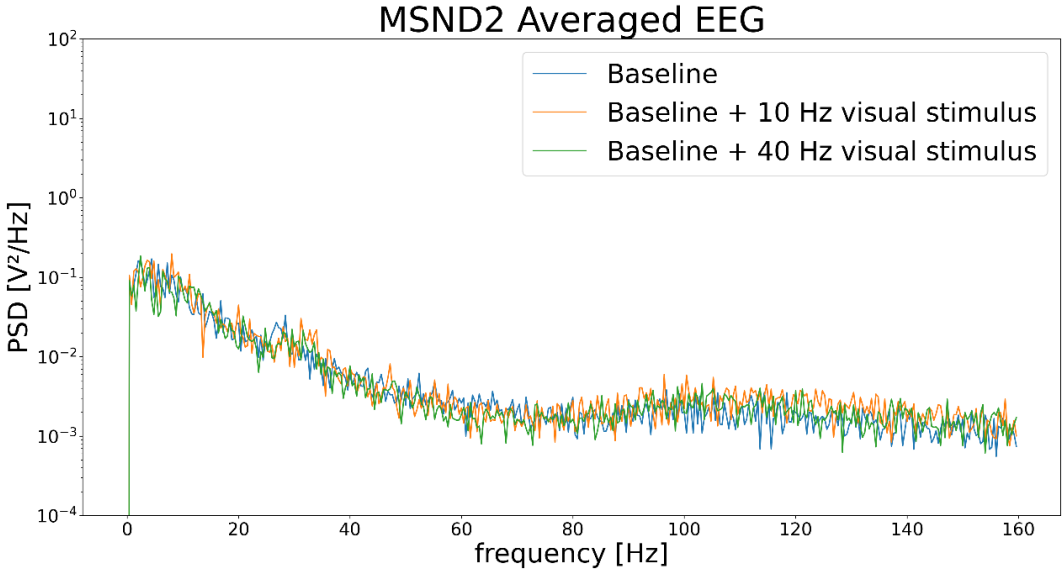

(b)

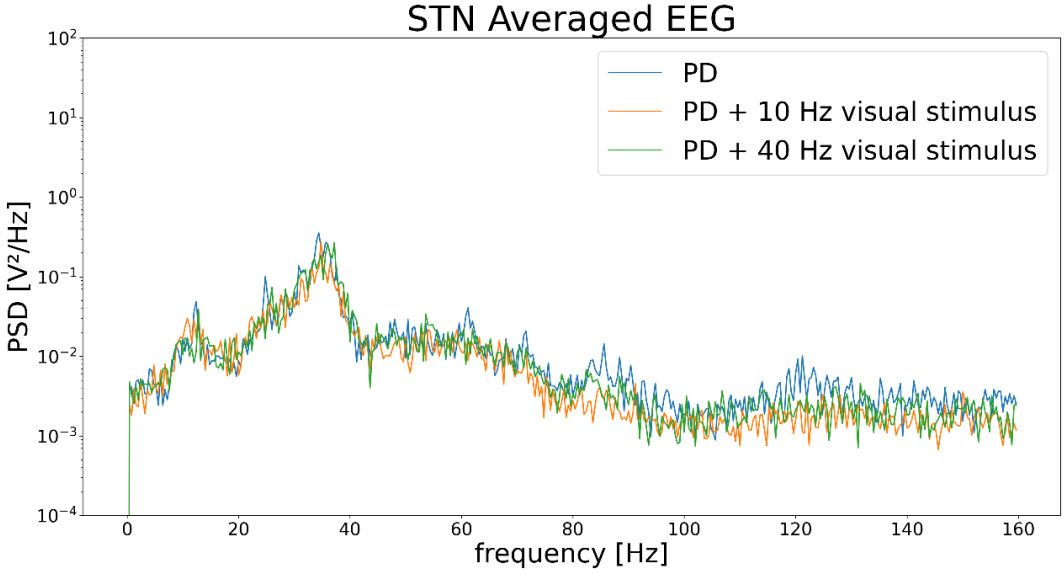

doi:10.6342/NTU202400853

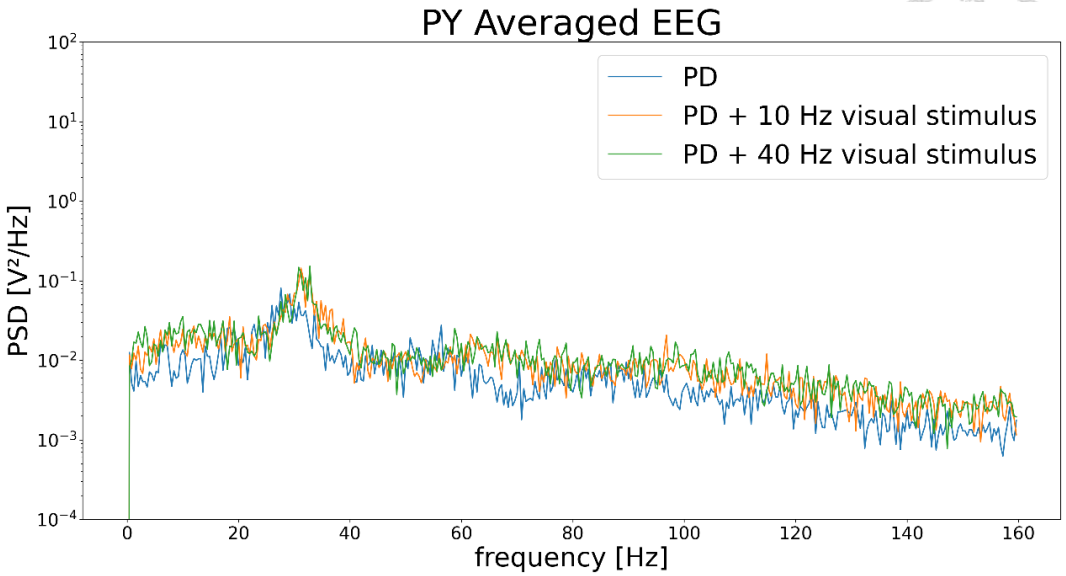

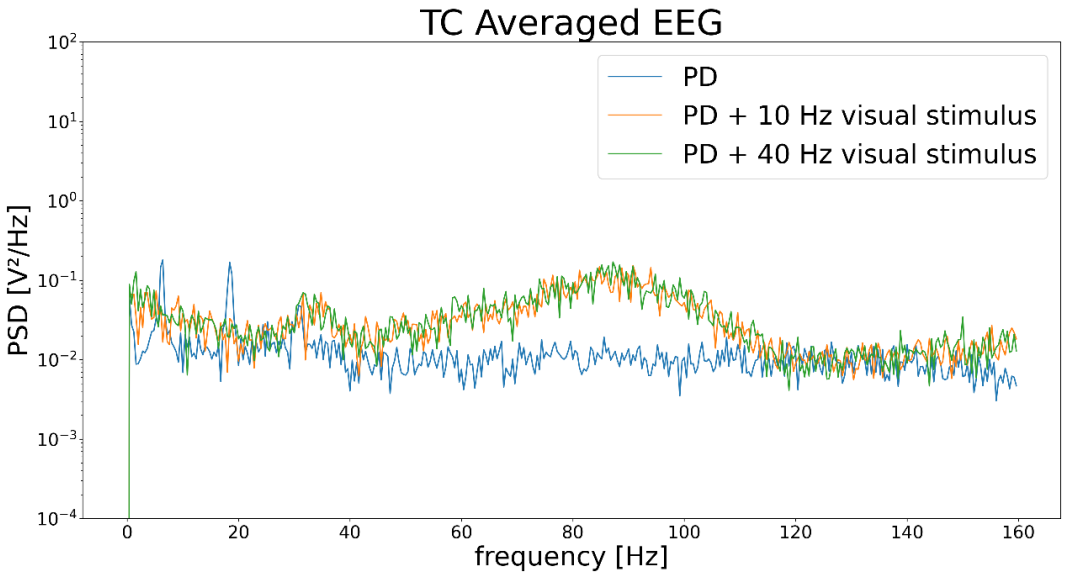

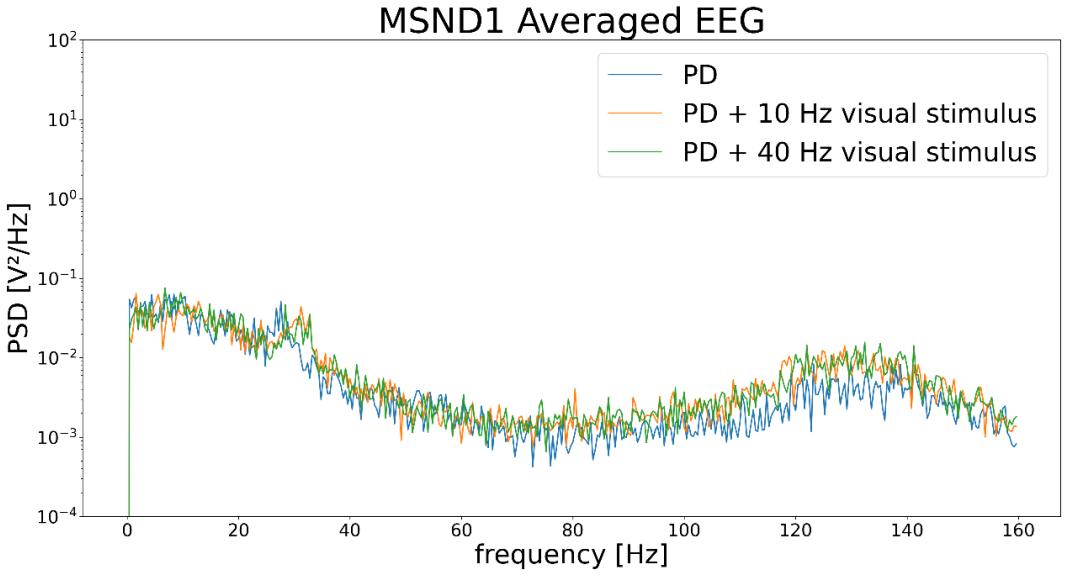

doi:10.6342/NTU202400853

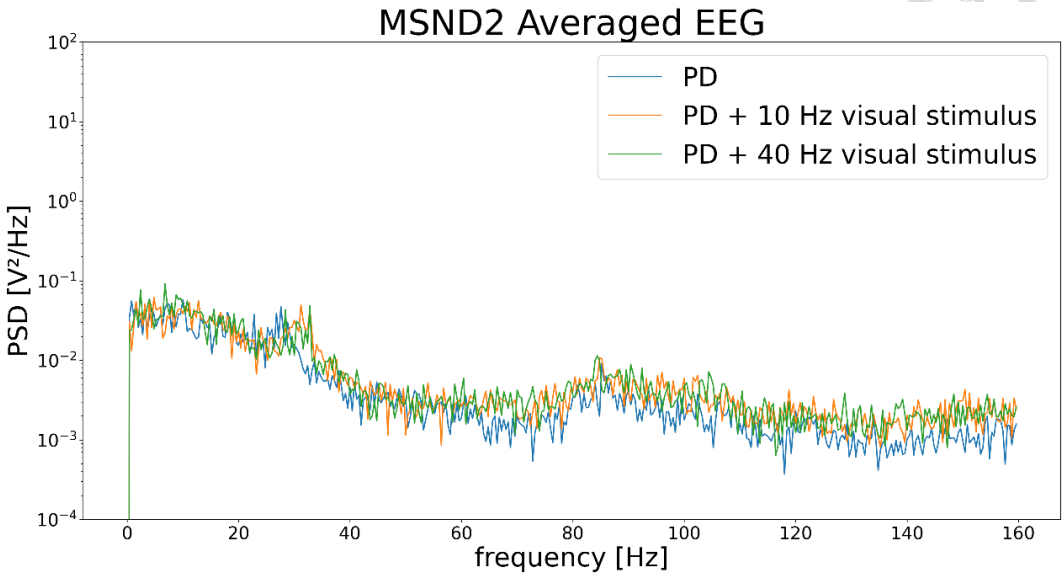

(c)

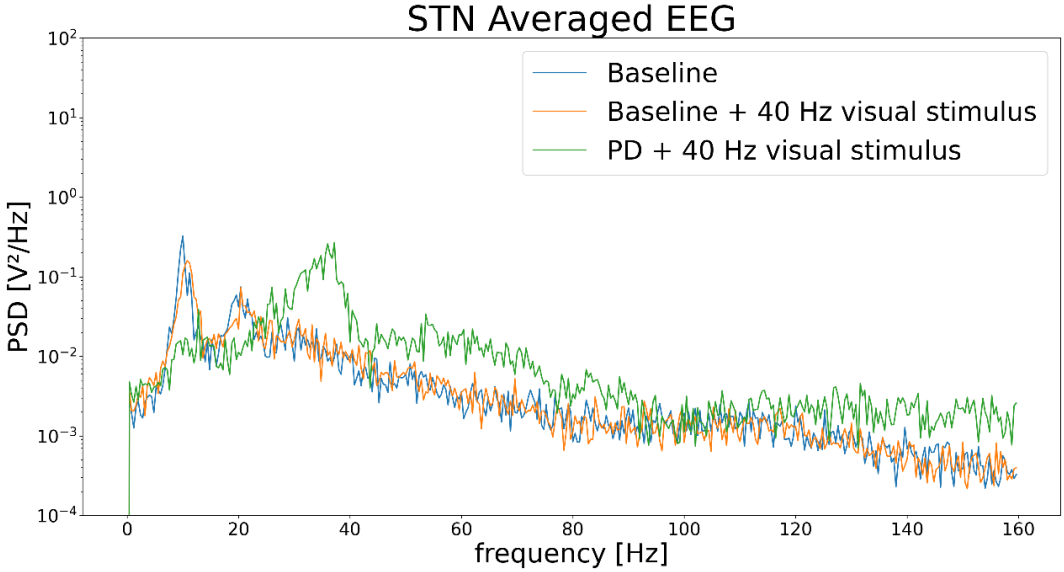

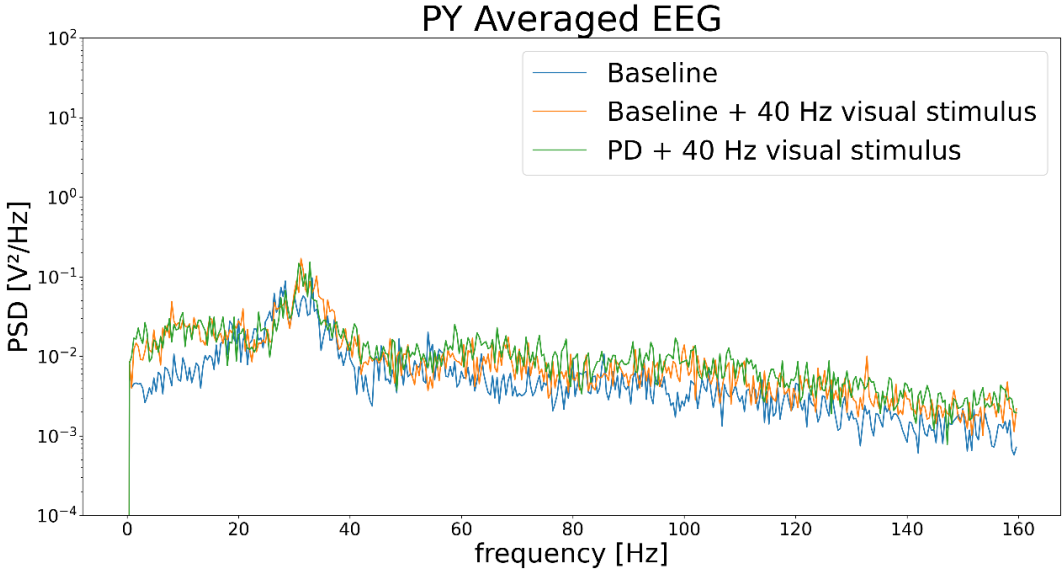

doi:10.6342/NTU202400853

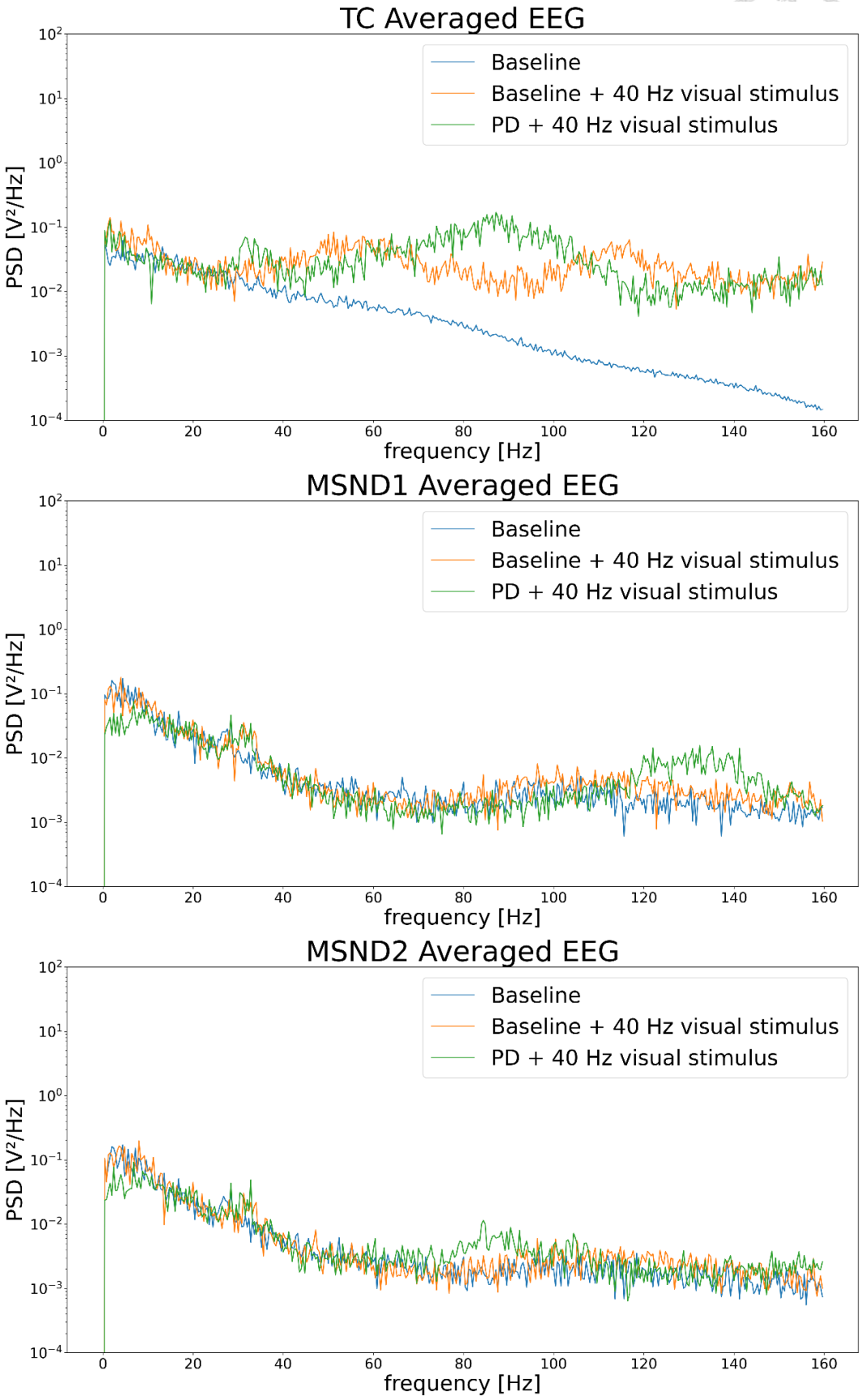

doi:10.6342/NTU202400853

(d)

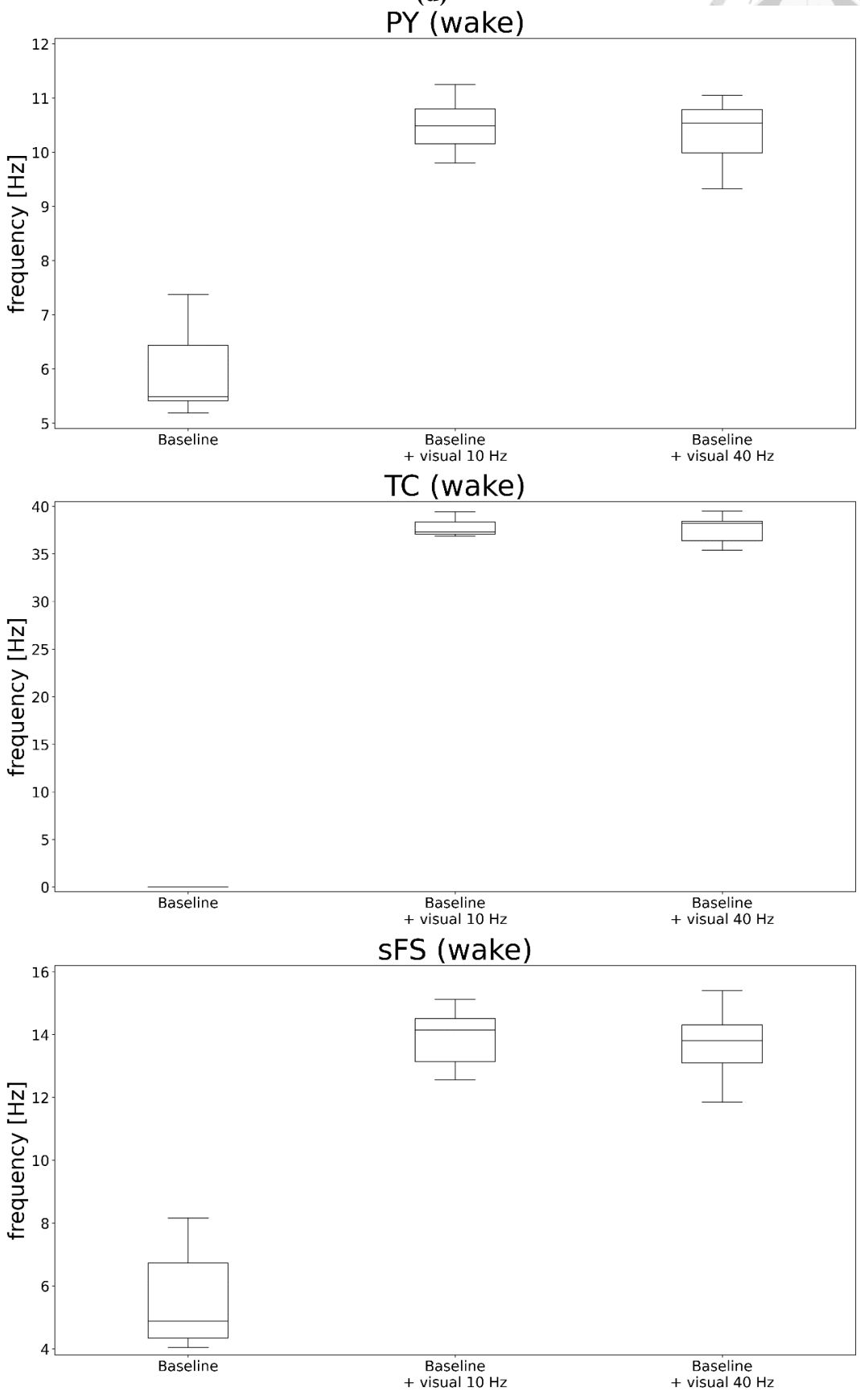

doi:10.6342/NTU202400853

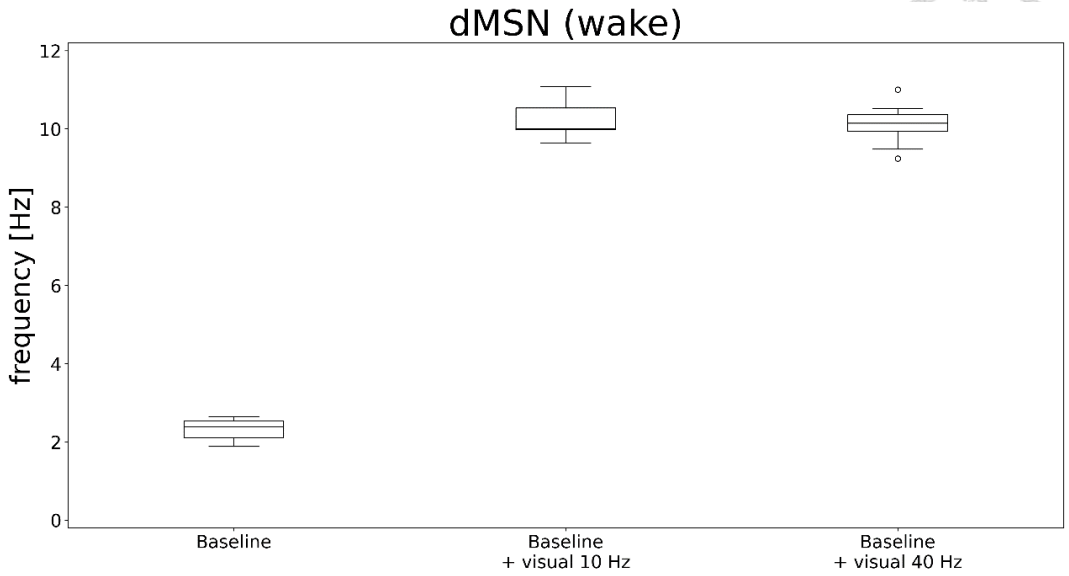

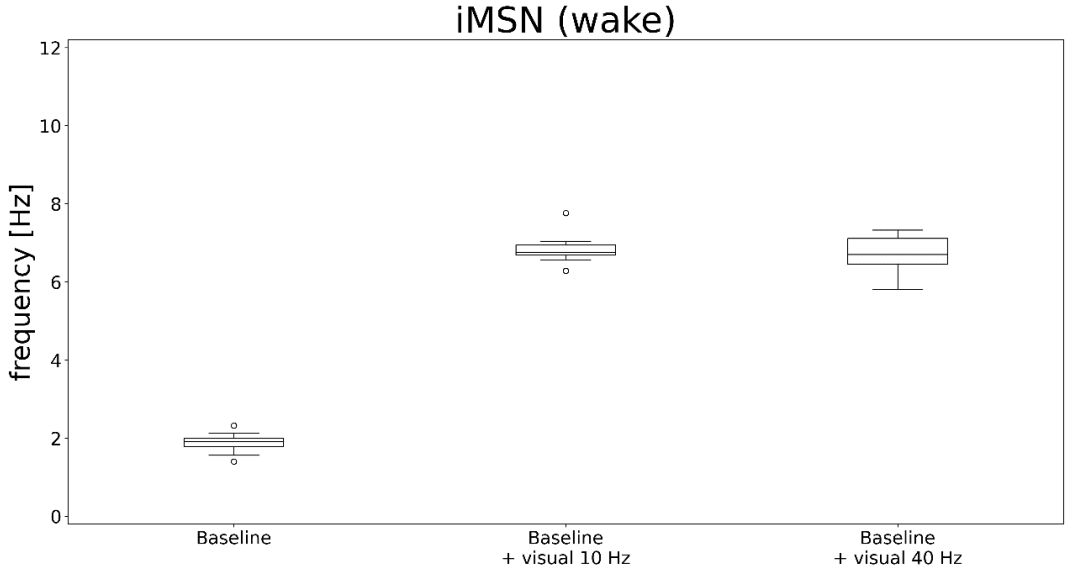

(e)

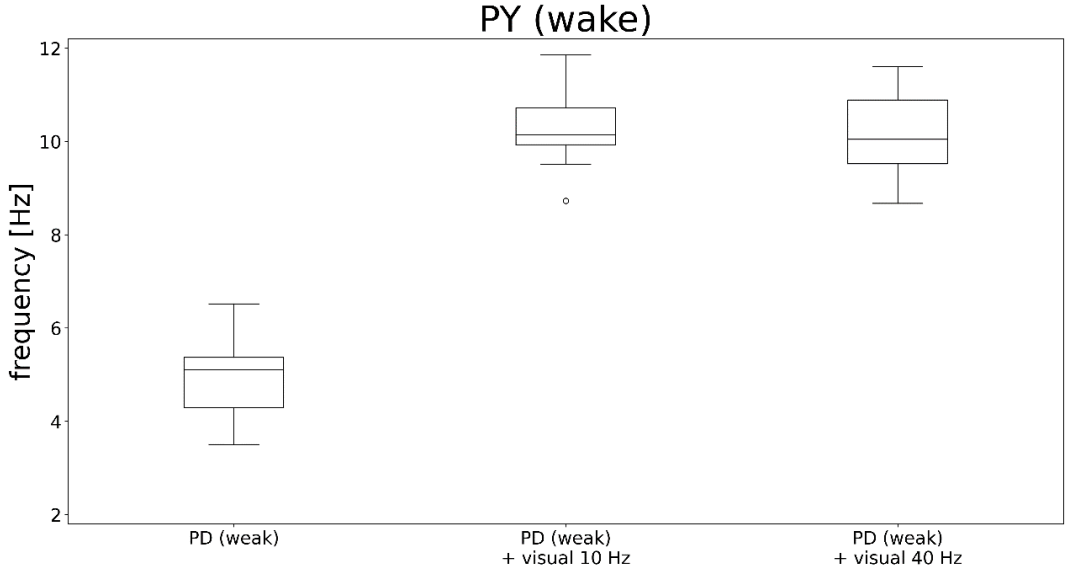

doi:10.6342/NTU202400853

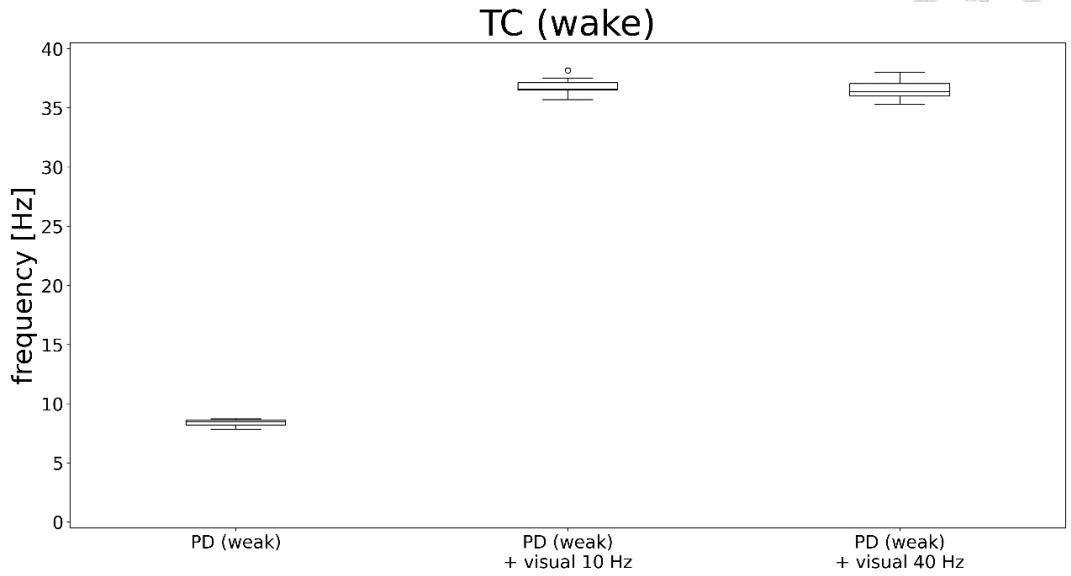

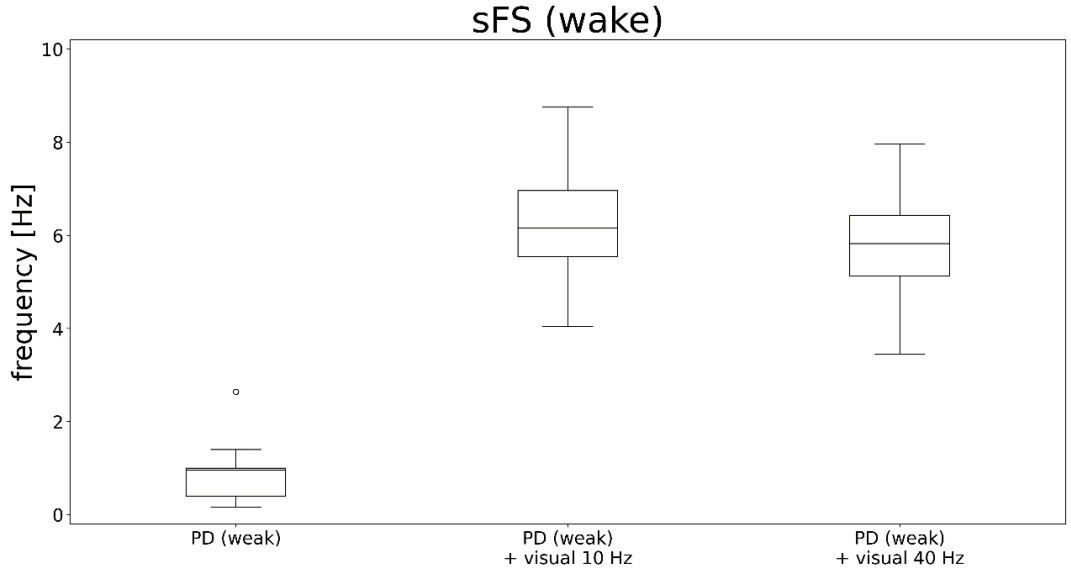

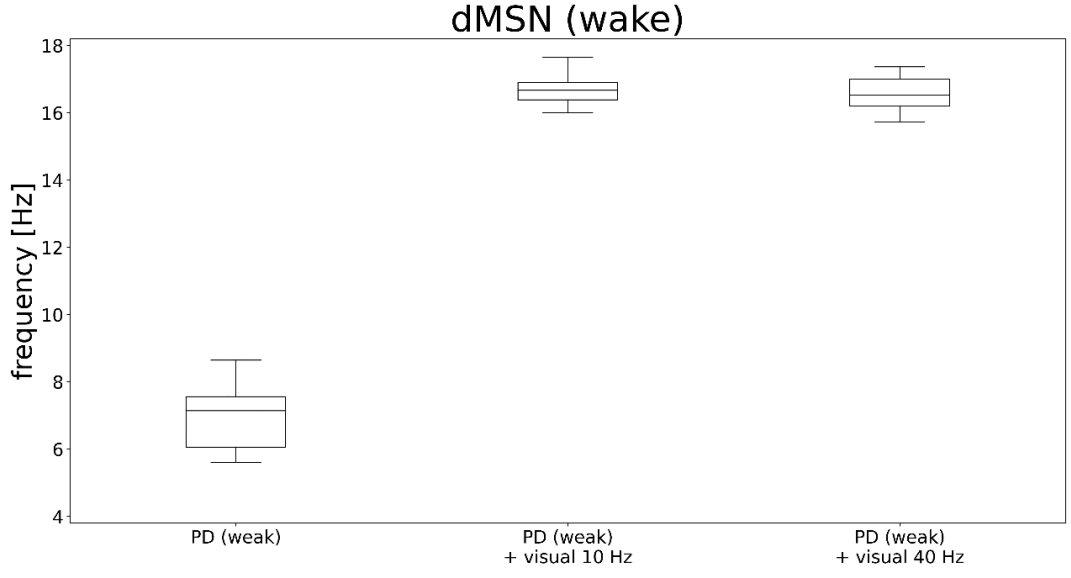

doi:10.6342/NTU202400853

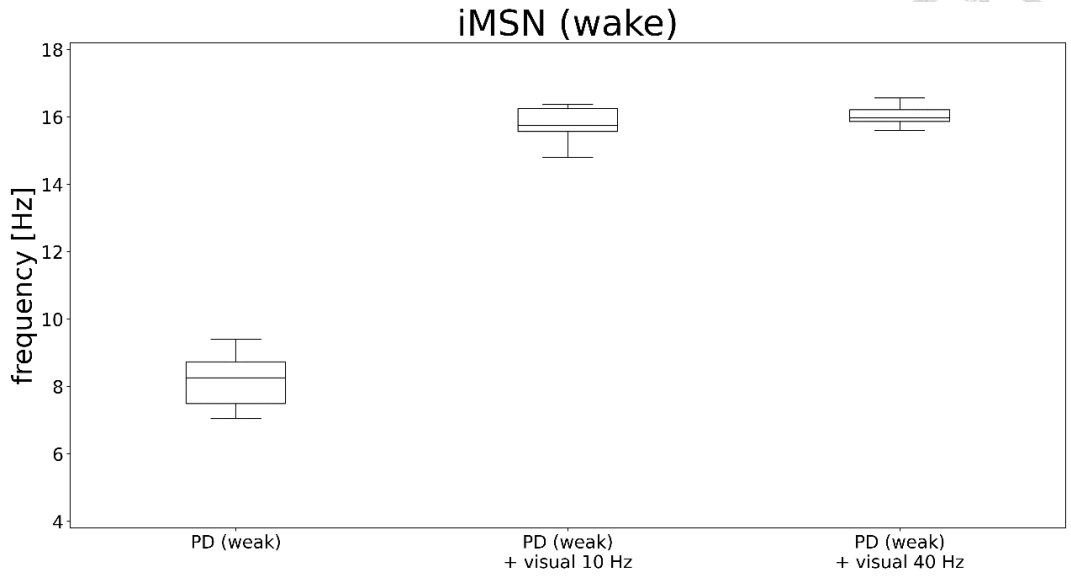

(f)

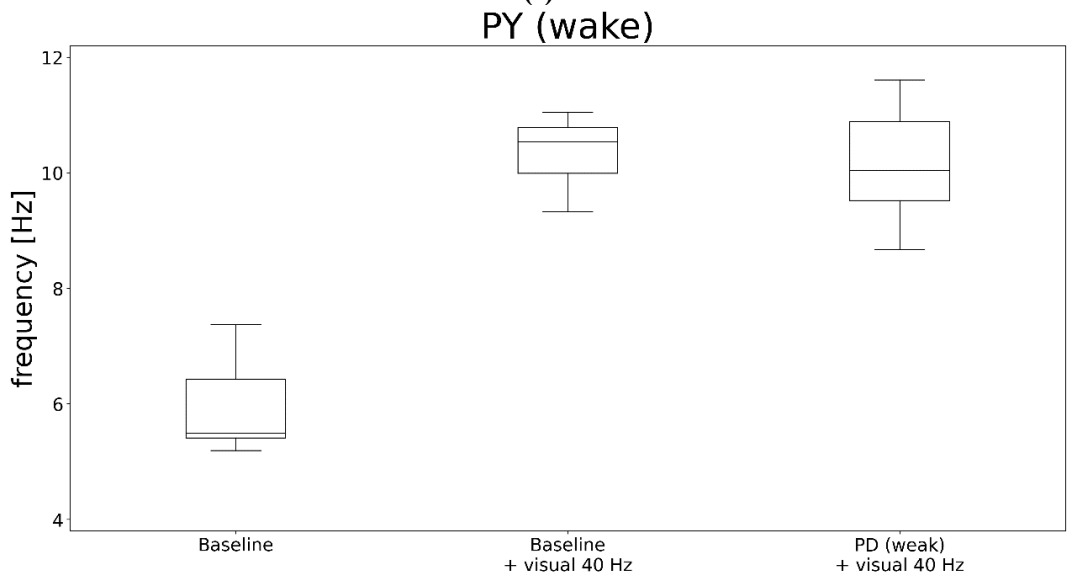

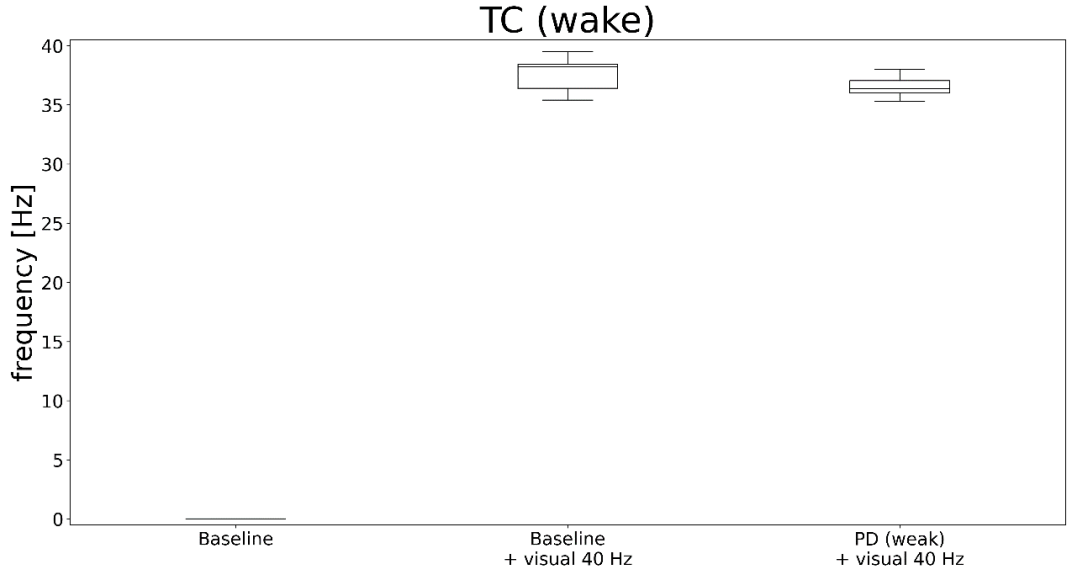

doi:10.6342/NTU202400853

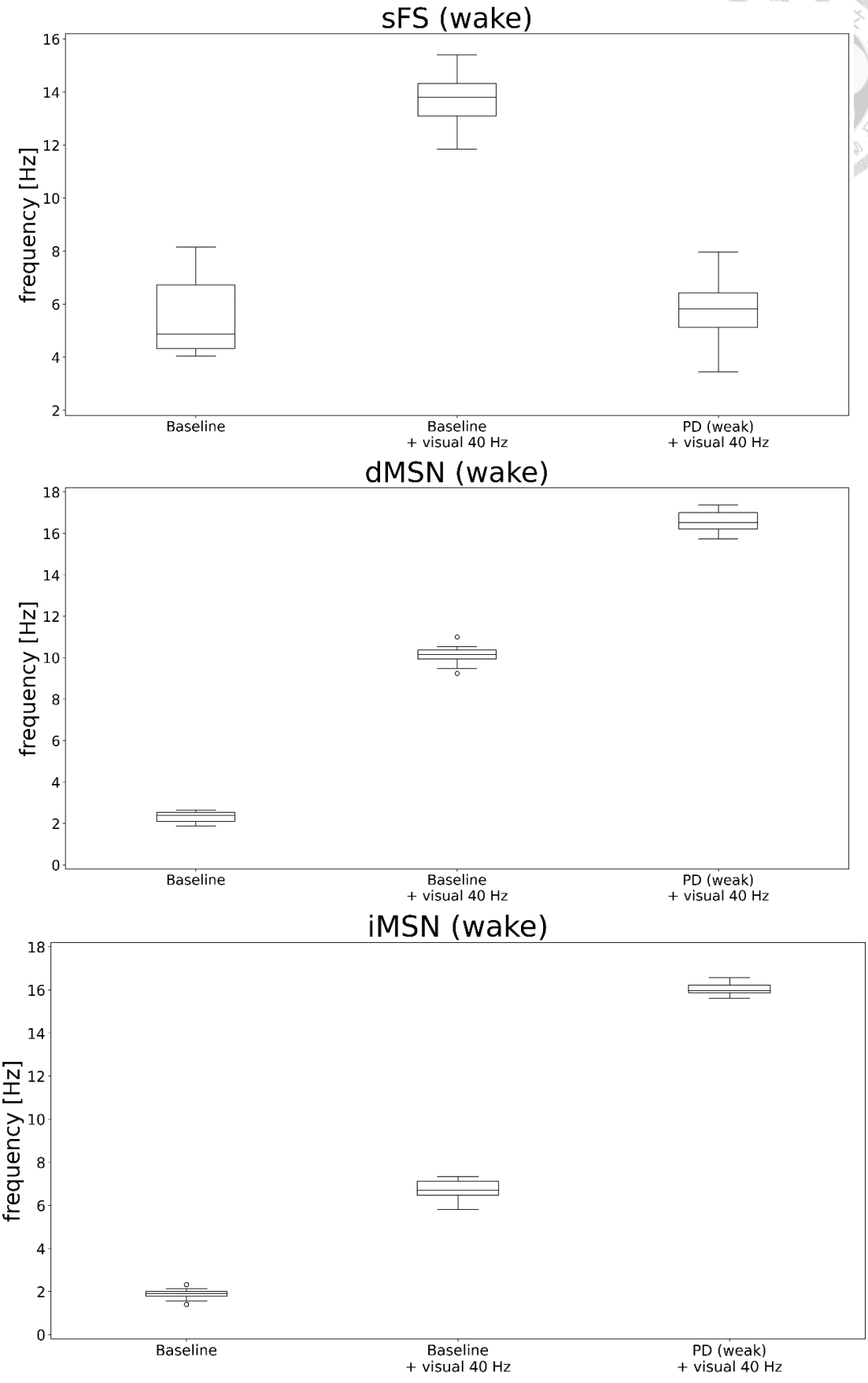

doi:10.6342/NTU202400853

Figure 8: Model under visual stimulation.

(a) PSD of neurons from top to down (STN, PY, TC, dMSN, iMSN) and from left to right (baseline, baseline + 10 Hz visual stimulation, baseline + 40 Hz visual stimulation). The X-axis is fixed at (0, 160), and the Y-axis is fixed at (1e-4, 1e+2).

(b) PSD of neurons from top to down (STN, PY, TC, dMSN, iMSN) and from left to right (baseline, weak PD, weak PD + 10 Hz visual stimulation, weak PD + 40 Hz visual stimulation). The X-axis is fixed at (0, 160), and the Y-axis is fixed at (1e-4, 1e+2).

(c) PSD of neurons from top to down (STN, PY, TC, dMSN, iMSN) and from left to right (baseline, baseline + 40 Hz visual stimulation, weak PD + 40 Hz visual stimulation). The X-axis is fixed at (0, 160), and the Y-axis is fixed at (1e-4, 1e+2).

(d) Firing frequency range of neurons from top to down (PY, TC, sFS, dMSN, iMSN) and from left to right (baseline, baseline + 10 Hz visual stimulation, baseline + 40 Hz visual stimulation).

(e) Firing frequency range of neurons from top to down (PY, TC, sFS, dMSN, iMSN) and from left to right (baseline, weak PD, weak PD + 10 Hz visual stimulation, weak PD + 40 Hz visual stimulation).

(f) Firing frequency range of neurons from top to down (PY, TC, sFS, dMSN, iMSN) and from left to right (baseline, baseline + 40 Hz visual stimulation, weak PD + 40 Hz visual stimulation).

doi:10.6342/NTU202400853

(a)

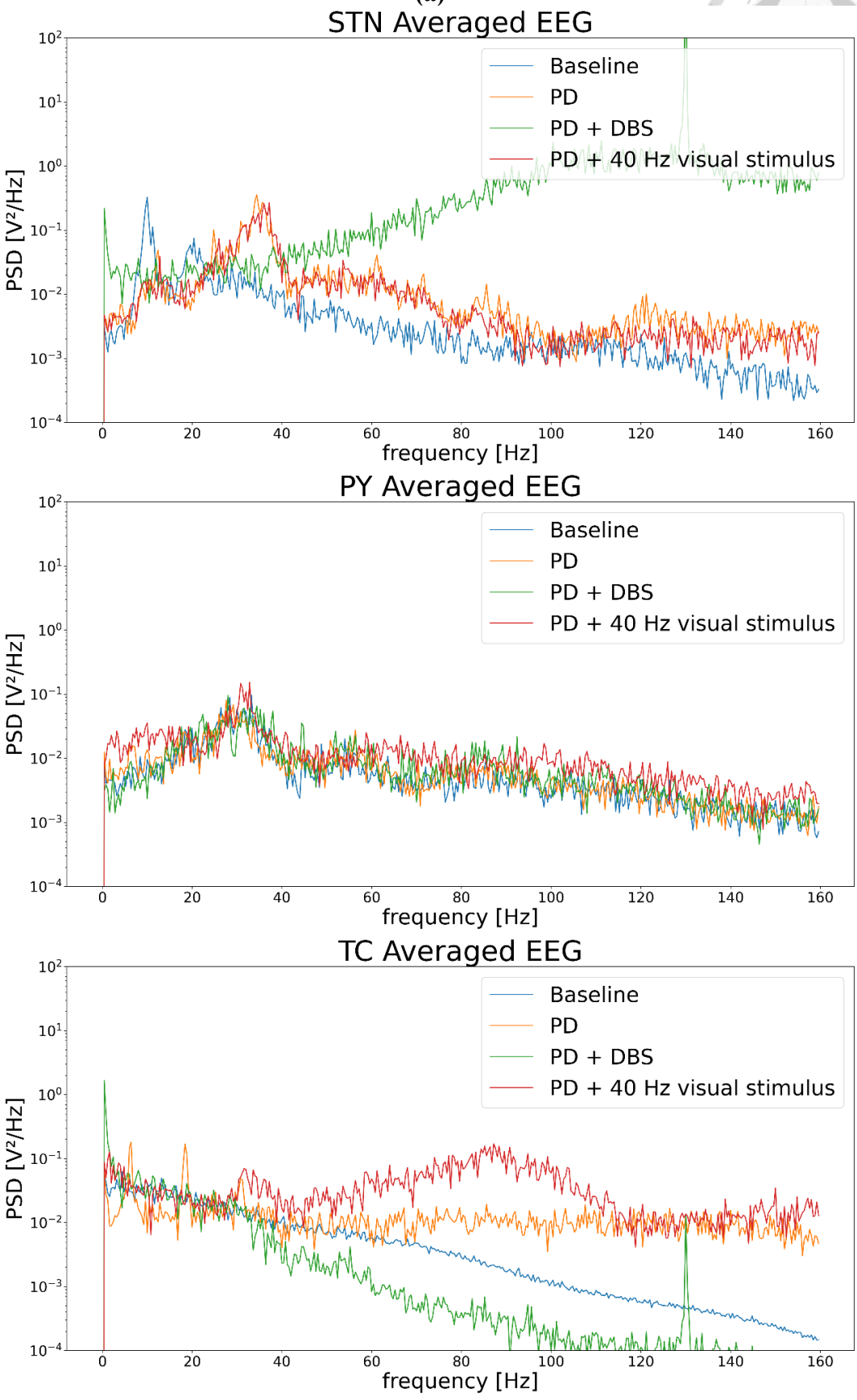

doi:10.6342/NTU202400853

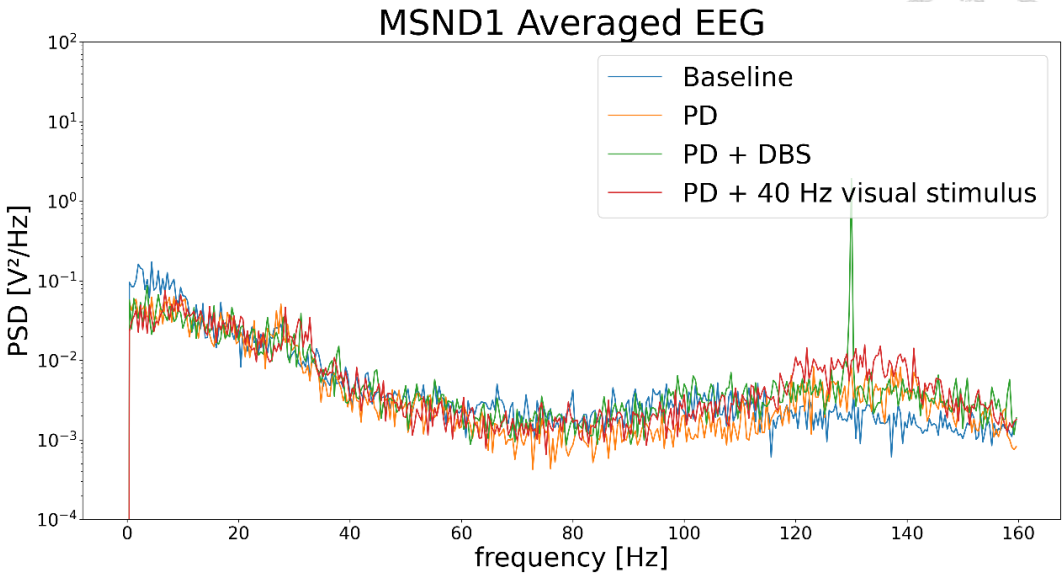

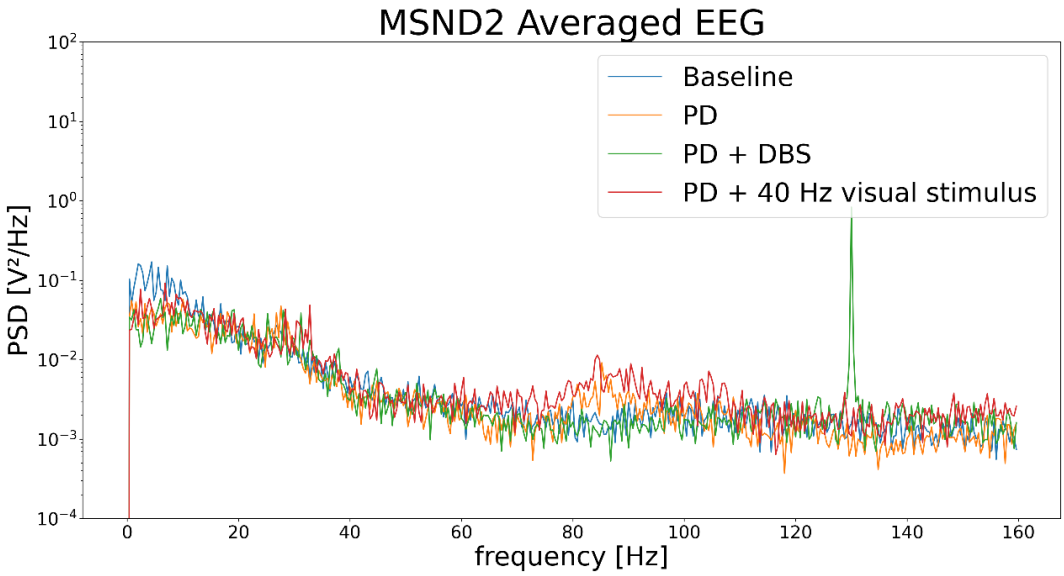

(b)

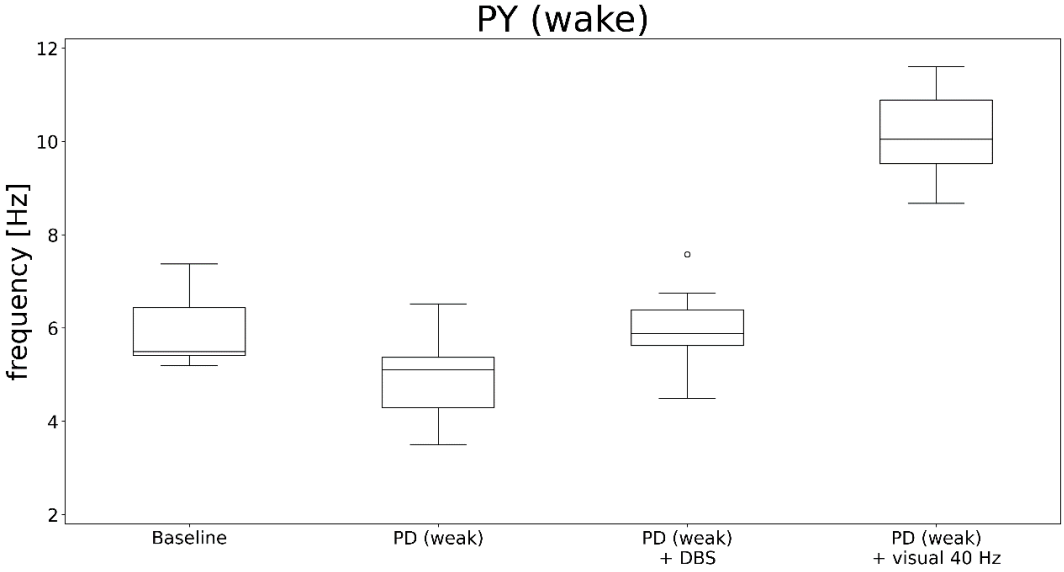

doi:10.6342/NTU202400853

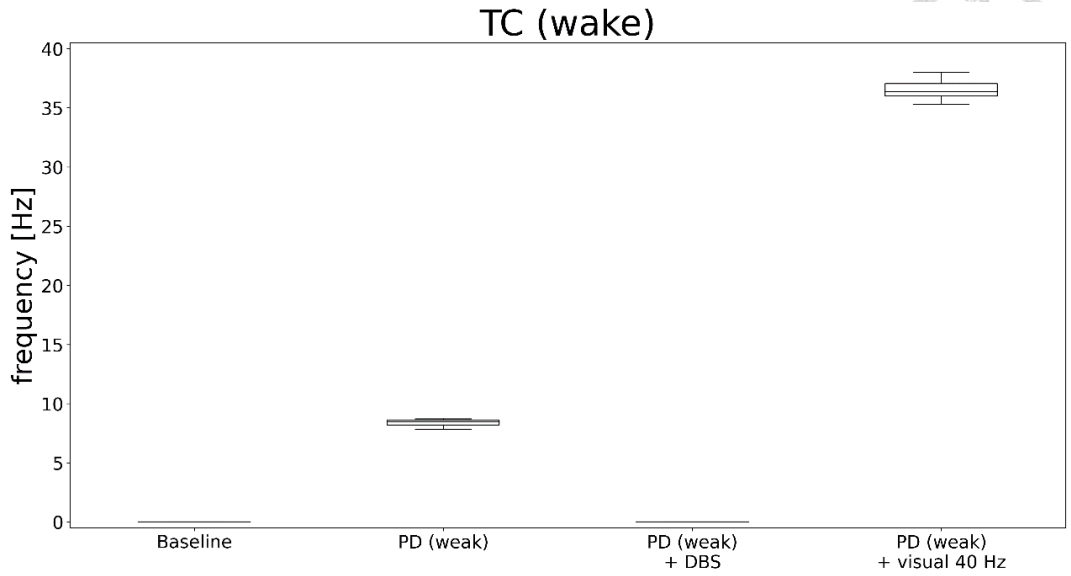

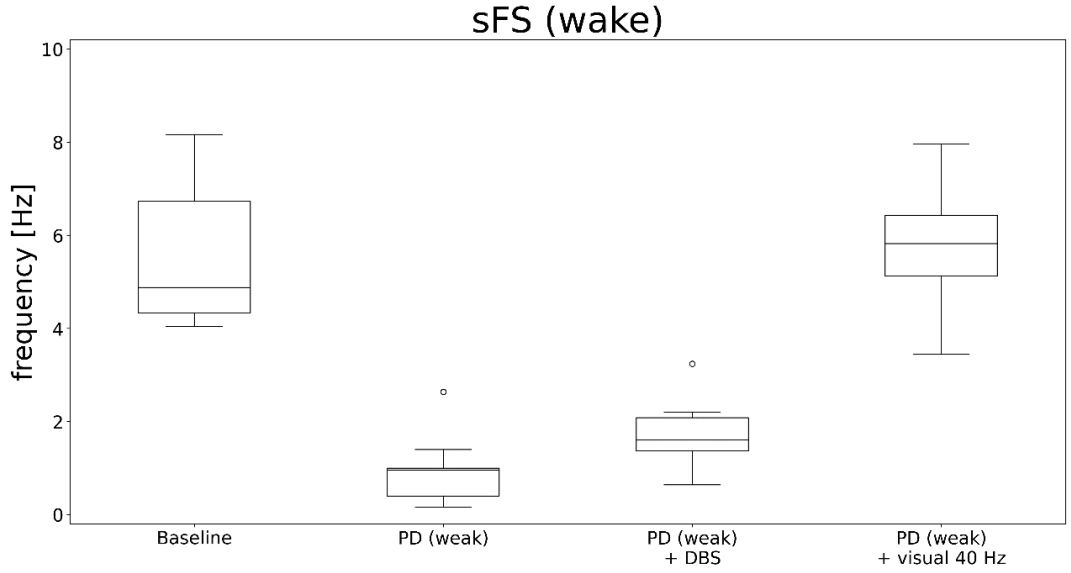

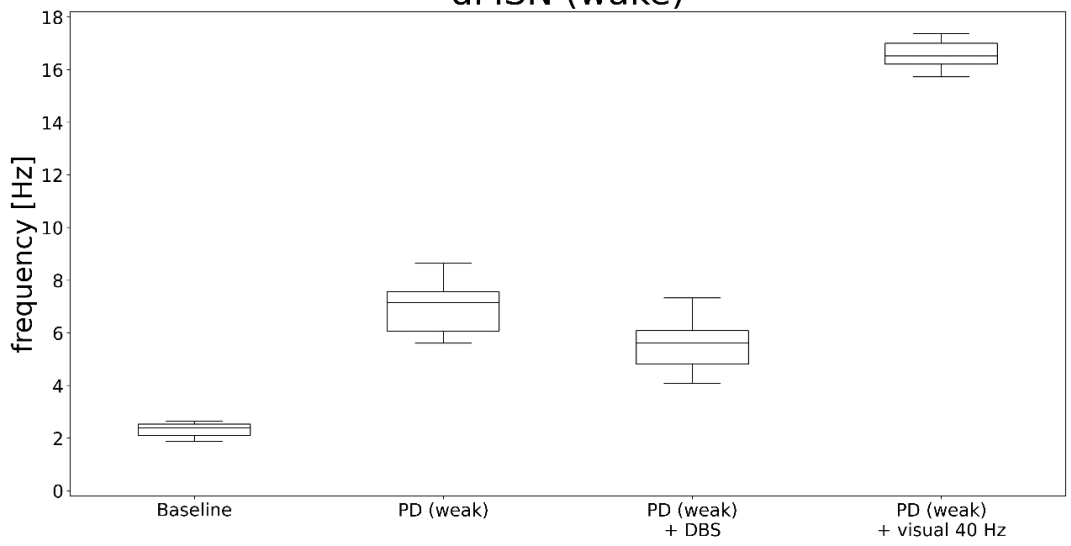

doi:10.6342/NTU202400853

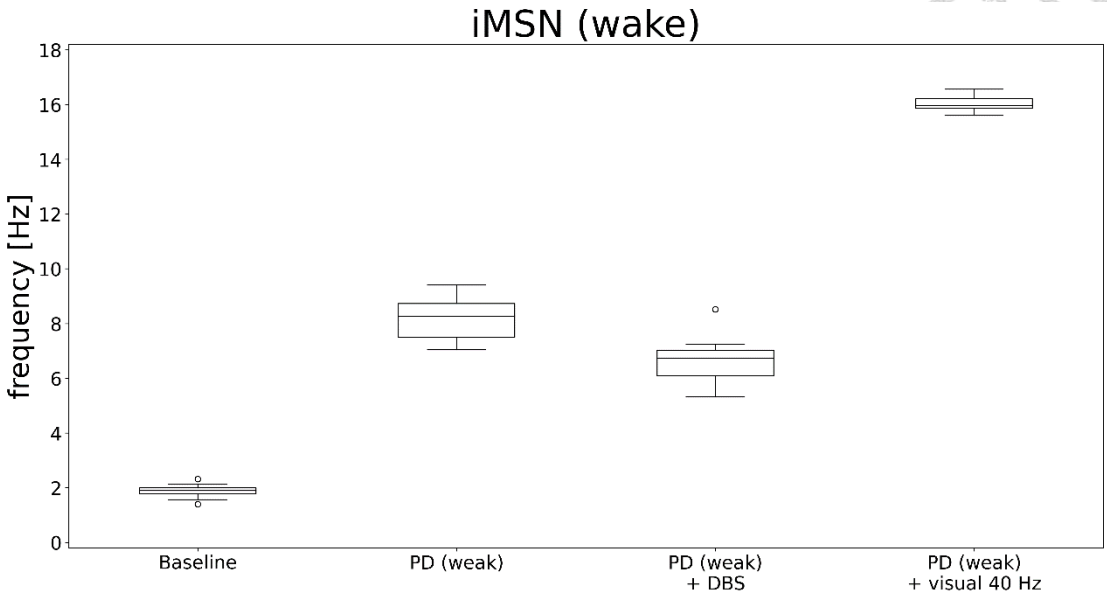

Figure 9: DBS versus 40 Hz visual stimulation in PD

(a) PSD of neurons from top to down (STN, PY, TC, dMSN, iMSN) and from left to right (baseline, weak PD, weak PD + 130 Hz DBS, weak PD + 40 Hz visual stimulation). The X-axis is fixed at (0, 160) and the Y-axis at (1e-4, 1e+2).

(b) Firing frequency range of neurons from top to down (PY, TC, sFS, dMSN, iMSN) and from left to right (baseline, weak PD, weak PD + 130 Hz DBS, weak PD + 40 Hz visual stimulation).

doi:10.6342/NTU202400853

Chapter 4 Discussion

Here, we build a whole HH neuron-based CBT model to simulate a combination of states, including PD progression state cross consciousness state. We have used a firing raster plot and PSD to verify the bridging model behaves as in separate models. We also compare how STN DBS and visual stimulation affect the CBT in PD in silico.

CBT loop can be affected by multiple anesthetic agents like propofol [45]. Propofol is used to induce and maintain general anesthesia by positive modulating the inhibiting GABAA receptor [46]. Jiang et al. [47] shows that the STN delta and theta power in DBS-treated patient in propofol anesthesia state is higher than in wake state. Our model in PD suggests elevated proportion of delta and theta power in propofol anesthesia state than in wake state (data not shown). Reports show that propofol can induce dyskinetic and dystonia [48], and our model might able to imply the side effects of propofol originate inside/outside the CBT loop. Besides, our model might serve as a filter of candidate anesthetic agents.

The therapeutic mechanism of DBS acts as a reversible lesion to block the propagation of the pathological beta wave [49]. Our model shows that STN DBS can block all signals, including pathological beta waves, to further propagate from TC to other downstream circuitry. Although the therapeutic mechanism of visual stimulation has not yet been cleared, Vanegas et al. [50] proposed that strong salient visual cues might overcome surrounding suppression and alleviate the freezing of gait episodes. Our model shows that visual stimulation can overcome the pathological beta wave in resting, wake TC, and propagate the desired signal to downstream circuitry. Together, our model

doi:10.6342/NTU202400853

suggests the effects of DBS and visual stimulus in normalizing dynamics and provides a validation model for future modification of therapeutic stimulation parameters.

This study has a few limitations. Firstly, Pathological beta wave reaches a plateau within ten days of administering MPTP to the rats [7]. As PD severity rises, we do not observe pathological beta power increases in our model. We expect that PD severity parameters space should constraint under weak PD state in order to observe the early PD CBT loop dynamics. Secondly, PY in all states has severely exaggerated high beta (20-30 Hz) synchronized and propagated through the whole network. However, the abnormal beta band does not disrupt the trend of pathological beta wave genesis in our model. While, it might influence further quantitative analysis. Finally, we do not observe pathological beta power in the PD/NREM state. NREM state is related to elevated maximum conductance of potassium leakage channel and eventually starts slow wave sleep (or NREM) [42], [43]. Therefore, the simulation of NREM cannot simply inject the duty cycle into the model as representative of the model.

doi:10.6342/NTU202400853

References

[1] T. R. Mhyre, J. T. Boyd, R. W. Hamill, and K. A. Maguire-Zeiss, "Parkinson's disease," *Subcell Biochem*, vol. 65, pp. 389–455, May 2012, doi: 10.1007/978-94-007-5416-4_16.

[2] GBD 2017 Disease and Injury Incidence and Prevalence Collaborators, "Global, regional, and national incidence, prevalence, and years lived with disability for 354 diseases and injuries for 195 countries and territories, 1990-2017: a systematic analysis for the Global Burden of Disease Study 2017.," *Lancet*, vol. 392, no. 10159, pp. 1789–1858, Nov. 2018, doi: 10.1016/S0140-6736(18)32279-7.

[3] Parkinson's Foundation, "Statistics | Parkinson's Foundation." Accessed: Jan. 26, 2024. [Online]. Available: https://www.parkinson.org/understanding-parkinsons/statistics

[4] 曾菁英,"台灣地區帕金森氏症之流行病學研究," 高雄醫學大學, 2007.

[5] A. Reeve, E. Simcox, and D. Turnbull, "Ageing and Parkinson's disease: why is advancing age the biggest risk factor?," *Ageing Res Rev*, vol. 14, no. 100, pp. 19–30, Mar. 2014, doi: 10.1016/j.arr.2014.01.004.

[6] M. M. McGregor and A. B. Nelson, "Circuit Mechanisms of Parkinson's Disease," *Neuron*, vol. 101, no. 6, pp. 1042–1056, Mar. 2019, doi: 10.1016/j.neuron.2019.03.004.

[7] N. Mallet, L. Delgado, M. Chazalon, C. Miguelez, and J. Baufreton, "Cellular and synaptic dysfunctions in Parkinson's disease: Stepping out of the striatum," *Cells*, vol. 8, no. 9. MDPI, Sep. 01, 2019. doi: 10.3390/cells8091005.

[8] J. Jankovic, "Parkinson's disease: clinical features and diagnosis," *J Neurol*

doi:10.6342/NTU202400853

Neurosurg Psychiatry, vol. 79, no. 4, pp. 368–376, Apr. 2008, doi: 10.1136/jnnp.2007.131045.

[9] National Institute of Neurological Disorders and Stroke (.gov), "Parkinson's Disease." Accessed: Jan. 26, 2024. [Online]. Available: https://www.ninds.nih.gov/health-information/disorders/parkinsons-disease

[10] J. Jankovic and L. G. Aguilar, "Current approaches to the treatment of Parkinson's disease.," *Neuropsychiatr Dis Treat*, vol. 4, no. 4, pp. 743–57, Aug. 2008, doi: 10.2147/ndt.s2006.

[11] P. Arias and J. Cudeiro, "Effects of rhythmic sensory stimulation (auditory, visual) on gait in Parkinson's disease patients," *Exp Brain Res*, vol. 186, no. 4, pp. 589–601, Apr. 2008, doi: 10.1007/s00221-007-1263-y.

[12] C. Adaikkan *et al.*, "Gamma Entrainment Binds Higher-Order Brain Regions and Offers Neuroprotection," *Neuron*, vol. 102, no. 5, pp. 929-943.e8, Jun. 2019, doi: 10.1016/j.neuron.2019.04.011.

[13] J. P. Gallivan and M. A. Goodale, "The dorsal 'action' pathway," 2018, pp. 449–466. doi: 10.1016/B978-0-444-63622-5.00023-1.

[14] N. N. Foster *et al.*, "The mouse cortico–basal ganglia–thalamic network," *Nature*, vol. 598, no. 7879, pp. 188–194, Oct. 2021, doi: 10.1038/s41586-021-03993-3.

[15] N. N. Foster *et al.*, "The mouse cortico–basal ganglia–thalamic network," *Nature*, vol. 598, no. 7879, pp. 188–194, Oct. 2021, doi: 10.1038/s41586-021-03993-3.

[16] C. Ghez and J. W. Krakauer, "Back 33 The Organization of Movement," 2006. [Online]. Available: https://api.semanticscholar.org/CorpusID:28725485

[17] R. Llinás, "Consciousness and the thalamocortical loop," *Int Congr Ser*, vol.

doi:10.6342/NTU202400853

1250, pp. 409–416, Oct. 2003, doi: 10.1016/S0531-5131(03)01067-7.

[18] W. H. R. Miltner, C. Braun, M. Arnold, H. Witte, and E. Taub, "Coherence of gamma-band EEG activity as a basis for associative learning," *Nature*, vol. 397, no. 6718, pp. 434–436, Feb. 1999, doi: 10.1038/17126.

[19] C. Tallon-Baudry, O. Bertrand, F. Peronnet, and J. Pernier, "Induced γ-Band Activity during the Delay of a Visual Short-Term Memory Task in Humans," *The Journal of Neuroscience*, vol. 18, no. 11, pp. 4244–4254, Jun. 1998, doi: 10.1523/JNEUROSCI.18-11-04244.1998.

[20] D. A. McCormick, M. J. McGinley, and D. B. Salkoff, "Brain state dependent activity in the cortex and thalamus," *Curr Opin Neurobiol*, vol. 31, pp. 133–140, Apr. 2015, doi: 10.1016/j.conb.2014.10.003.

[21] A. D. Mizrahi-Kliger, A. Kaplan, Z. Israel, M. Deffains, and H. Bergman, "Basal ganglia beta oscillations during sleep underlie Parkinsonian insomnia," *Proc Natl Acad Sci U S A*, vol. 117, no. 29, pp. 17359–17368, Jul. 2020, doi: 10.1073/pnas.2001560117.

[22] E. Ahissar, G. Nelinger, E. Assa, O. Karp, and I. Saraf-Sinik, "Thalamocortical loops as temporal demodulators across senses," *Commun Biol*, vol. 6, no. 1, p. 562, May 2023, doi: 10.1038/s42003-023-04881-4.

[23] S. Ching, A. Cimenser, P. L. Purdon, E. N. Brown, and N. J. Kopell, "Thalamocortical model for a propofol-induced α-rhythm associated with loss of consciousness," *Proc Natl Acad Sci U S A*, vol. 107, no. 52, pp. 22665–22670, Dec. 2010, doi: 10.1073/pnas.1017069108.

[24] K. Azdad *et al.*, "Homeostatic Plasticity of Striatal Neurons Intrinsic Excitability following Dopamine Depletion," *PLoS One*, vol. 4, no. 9, p. e6908, Sep. 2009, doi: 10.1371/journal.pone.0006908.

doi:10.6342/NTU202400853

[25] D. J. Surmeier, “To go or not to go,” *Nature*, vol. 494, no. 7436, pp. 178–179, Feb. 2013, doi: 10.1038/nature11856.

[26] M. S. Patton, M. Heckman, C. Kim, C. Mu, and B. N. Mathur, “Compulsive alcohol consumption is regulated by dorsal striatum fast-spiking interneurons,” *Neuropsychopharmacology*, vol. 46, no. 2, pp. 351–359, Jan. 2021, doi: 10.1038/s41386-020-0766-0.

[27] K. C. Luk and A. F. Sadikot, “GABA promotes survival but not proliferation of parvalbumin-immunoreactive interneurons in rodent neostriatum: an in vivo study with stereology,” *Neuroscience*, vol. 104, no. 1, pp. 93–103, Apr. 2001, doi: 10.1016/S0306-4522(01)00038-0.

[28] Y. Kawaguchi, “Physiological, morphological, and histochemical characterization of three classes of interneurons in rat neostriatum,” *The Journal of Neuroscience*, vol. 13, no. 11, pp. 4908–4923, Nov. 1993, doi: 10.1523/JNEUROSCI.13-11-04908.1993.

[29] S. Zhai, W. Shen, S. M. Graves, and D. J. Surmeier, “Dopaminergic modulation of striatal function and Parkinson’s disease,” *J Neural Transm*, vol. 126, no. 4, pp. 411–422, Apr. 2019, doi: 10.1007/s00702-019-01997-y.

[30] Mallet, Delgado, Chazalon, Miguelez, and Baufreton, “Cellular and Synaptic Dysfunctions in Parkinson’s Disease: Stepping out of the Striatum,” *Cells*, vol. 8, no. 9, p. 1005, Aug. 2019, doi: 10.3390/cells8091005.

[31] M. M. McGregor and A. B. Nelson, “Circuit Mechanisms of Parkinson’s Disease,” *Neuron*, vol. 101, no. 6, pp. 1042–1056, Mar. 2019, doi: 10.1016/j.neuron.2019.03.004.

[32] Michael H. Grider; Rishita Jessu; Rian Kabir., “Physiology, Action Potential.” Accessed: Jan. 26, 2024. [Online]. Available:

doi:10.6342/NTU202400853

https://www.ncbi.nlm.nih.gov/books/NBK538143/

[33] S. Alexander, A. Mathie, and J. Peters, “ION CHANNELS,” *Br J Pharmacol*, vol. 164, no. s1, Nov. 2011, doi: 10.1111/j.1476-5381.2011.01649_5.x.

[34] R. Dermietzel and D. C. Spray, “Gap Junctions, Electric Synapses,” in *Neuroscience in the 21st Century*, New York, NY: Springer New York, 2013, pp. 439–473. doi: 10.1007/978-1-4614-1997-6_18.

[35] A. L. HODGKIN and A. F. HUXLEY, “A quantitative description of membrane current and its application to conduction and excitation in nerve.,” *J Physiol*, vol. 117, no. 4, pp. 500–44, Aug. 1952, doi: 10.1113/jphysiol.1952.sp004764.

[36] Y. Yu and Q. Wang, “Oscillation dynamics in an extended model of thalamic-basal ganglia,” *Nonlinear Dyn*, vol. 98, no. 2, pp. 1065–1080, Oct. 2019, doi: 10.1007/s11071-019-05249-2.

[37] S. Sasi and B. Sen Bhattacharya, “Phase entrainment by periodic stimuli in silico: A quantitative study,” *Neurocomputing*, vol. 469, pp. 273–288, Jan. 2022, doi: 10.1016/j.neucom.2021.10.077.

[38] 卓嘉虹, “基於強化學習和基底核-丘腦動態網路之帕金森氏症閉迴路深腦電刺激演算法,” 國立臺灣大學, 2022. doi: 10.6342/NTU202200118.

[39] N. Kim, J. W. Barter, T. Sukharnikova, and H. H. Yin, “Striatal firing rate reflects head movement velocity,” *European Journal of Neuroscience*, vol. 40, no. 10, pp. 3481–3490, Nov. 2014, doi: 10.1111/ejn.12722.

[40] E. M. Adam, E. N. Brown, N. Kopell, and M. M. Mccarthy, “Deep brain stimulation in the subthalamic nucleus for Parkinson’s disease can restore dynamics of striatal networks,” 2023, doi: 10.1073/pnas.

[41] M. M. McCarthy, E. N. Brown, and N. Kopell, “Potential network mechanisms

doi:10.6342/NTU202400853

mediating electroencephalographic beta rhythm changes during propofol-induced paradoxical excitation," *Journal of Neuroscience*, vol. 28, no. 50, pp. 13488–13504, Dec. 2008, doi: 10.1523/JNEUROSCI.3536-08.2008.

[42] S. Hill and G. Tononi, "Modeling Sleep and Wakefulness in the Thalamocortical System," *J Neurophysiol*, vol. 93, no. 3, pp. 1671–1698, Mar. 2005, doi: 10.1152/jn.00915.2004.

[43] K. Yoshida, S. Shi, M. Ukai-Tadenuma, H. Fujishima, R. Ohno, and H. R. Ueda, "Leak potassium channels regulate sleep duration," *Proceedings of the National Academy of Sciences*, vol. 115, no. 40, Oct. 2018, doi: 10.1073/pnas.1806486115.

[44] E. Lumer, "Neural dynamics in a model of the thalamocortical system. I. Layers, loops and the emergence of fast synchronous rhythms," *Cerebral Cortex*, vol. 7, no. 3, pp. 207–227, Apr. 1997, doi: 10.1093/cercor/7.3.207.

[45] S. Shaikh and H. Verma, "Parkinson′s disease and anaesthesia," *Indian J Anaesth*, vol. 55, no. 3, p. 228, 2011, doi: 10.4103/0019-5049.82658.

[46] S. Adodra and T. G. Hales, "Potentiation, activation and blockade of $GABA_A$ receptors of clonal murine hypothalamic GT1-7 neurones by propofol," *Br J Pharmacol*, vol. 115, no. 6, pp. 953–960, Jul. 1995, doi: 10.1111/j.1476-5381.1995.tb15903.x.

[47] N. Jiang *et al.*, "Optimized Propofol Anesthesia Increases Power of Subthalamic Neuronal Activity in Patients with Parkinson's Disease Undergoing Deep Brain Stimulation," *Neurol Ther*, vol. 10, no. 2, pp. 785–802, Dec. 2021, doi: 10.1007/s40120-021-00259-y.

[48] D. P. Roberts and S. J. G. Lewis, "Considerations for general anaesthesia in Parkinson's disease," *Journal of Clinical Neuroscience*, vol. 48, pp. 34–41, Feb.

doi:10.6342/NTU202400853

2018, doi: 10.1016/j.jocn.2017.10.062.

[49] T. M. Herrington, J. J. Cheng, and E. N. Eskandar, “Mechanisms of deep brain stimulation,” *J Neurophysiol*, vol. 115, no. 1, pp. 19–38, Jan. 2016, doi: 10.1152/jn.00281.2015.

[50] M. I. Vanegas *et al.*, “Altered dynamics of visual contextual interactions in Parkinson’s disease,” *NPJ Parkinsons Dis*, vol. 5, no. 1, p. 13, Jul. 2019, doi: 10.1038/s41531-019-0085-5.

doi:10.6342/NTU202400853